Lehigh University
Lehigh Preserve

Theses and Dissertations

2012

Thermal Effects on Restoring Force and Dielectric Charge Density of RF MEMS Switch

Guosong Zeng
Lehigh University

Follow this and additional works at: http://preserve.lehigh.edu/etd

Recommended Citation
Zeng, Guosong, "Thermal Effects on Restoring Force and Dielectric Charge Density of RF MEMS Switch" (2012). *Theses and Dissertations.* Paper 1366.

This Thesis is brought to you for free and open access by Lehigh Preserve. It has been accepted for inclusion in Theses and Dissertations by an authorized administrator of Lehigh Preserve. For more information, please contact preserve@lehigh.edu.

THERMAL EFFECTS ON RESTORING FORCE AND DIELECTRIC CHARGE DENSITY OF RF MEMS SWITCH

by

Guosong Zeng

A Thesis

Presented to the Graduate and Research Committee

of Lehigh University

in Candidacy for the Degree of

Master of Science

in

The Department of Mechanical Engineering and Mechanics

Lehigh University

May, 2012

This thesis is accepted and approved in partial fulfillment of the requirements for the Master of Science.

____

Date

____

Herman F. Nied, Ph. D.

Thesis Advisor

____

D. Gary Harlow, Ph. D.

Chairperson of Department

Acknowledgements

I would like to thank my advisor Prof. Herman F. Nied, who gave me many valuable opinions and help during my thesis. Under his instruction, I accomplished the simulation of the RF MEMS switch structure, and obtained some desired results, which will be very helpful for future studies. Working with him is so unforgettable, and I really learn a lot of things during this period of time. I would also like to thank Prof. Nied for his supporting my PhD application. Without his help, it is impossible for me to apply to the group which I am interested in.

I would thank to Prof. Espinosa, and Prof. Zhu, from Northwestern University and North Carolina State University, respectively, who gave me many helpful suggestions.

I would thank to Dr. Xiaofeng Zhang from Tianjin University, who gave me so many advises in my simulation.

I would like to thank to Dr. Cristiano Palego and Mr. Guanghai Ding, who spent so much time discussing the calculation of the charge density with me.

I would like to thank to Mr. Haolin Ma, Mr. Yi Chen, Mr. Qi Zhang, Mr. Yunlong Kang, Mr. Yuzhong Zheng and some other friends, for their friendly support and companionship.

I am also thankful to Mrs. JoAnn Casciano for her administrative assistance.

Finally, I want to thank to my parents and my girl friend Miss. Mengni Cao. It is impossible for me to achieve my goal without your support and love.

Contents

TITLE I
Acknowledgements IV
List of Tables VIII
List of Figures IX
Abstract 1
1 Introduction 2
1.1 Micro/Nanotechnology 2
1.1.1 Category of Micro/Nanotechnology 4
1.2 Brief Introduction to MEMS 6
1.2.1 Category of MEMS 7
1.2.2 Characteristics of MEMS 10
1.2.3 Present Situation of MEMS industry 12
1.3 RF MEMS Technology 12
1.3.1 Configuration of RF MEMS 13
1.3.2 RF MEMS Advantages 14
1.4 RF MEMS Switch 15
1.5 Structure of Thesis 20
2 Basic Mechanical Behavior of RF MEMS Switches 21
2.1 Mechanical Model of Electrostatic Actuation RF MEMS Switches 21
2.1.1 Static State Mechanical Characteristics of Electrostatic Actuation RF MEMS Capacitive Switch 21
2.1.2 Dynamic Analysis of the Mechanical Characteristics of Electrostatic Actuation RF MEMS Switch 25
2.2 Failure Phenomenon of RF MEMS Switches 28
2.2.1 Stiction Effect in DC-Contact MEMS Switch 28
2.2.2 Buckling Deformation Effect in DC-Contact MEMS Switch 31
3 Thermal Effects on Switches Reliability 33
3.1 Low Temperature Effects on RF MEMS Switches 33
3.2 High Temperature Effects on RF MEMS Switches 35
4 Thermoelasticity Analysis 39
4.1 Thermoelastic Theory 40
4.2 Finite Element Method 43

4.3 ANSYS Simulation 45
5 Finite Element Modeling of Thermal Stresses in Membranes 48
5.1 Finite Element Modeling of Membrane Thermal Stress 49
5.2 Analytical Model of release voltage of RF MEMS Switches 61
5.3 The Effects of Dielectric Layer Geometry on RF MEMS Switch Capacitance 67
6 Conclusion and Future Work 80
Appendix 83
Reference 86
Vita 95

List of Tables

Table.1-1 Performance comparison of RF MEMS switch, FET and PIN transistor…….16

Table.5-1 Critical parameters of RF MEMS membrane (Au)……………………………........50

Table.5-2 Young`s modulus of Au in different temperature………………………………...51

Table.App-1Elastic Modulus……………………………………………………………………..83

Table.App-2 Calculation of coefficients of polynomial…………………………………84

List of Figures

Fig.1-1 Moore`s law and the counts of microdevices from 1971-2011…………………..3

Fig.1-2-1 ADXL202 micro-acceleration sensor………………………………………….8

Fig.1-2-2micro-electrostatic motor……………………………………………………….9

Fig.1-3-1 Scanning electron microscope photograph of a MEMS switch, showing the source, gate and drain………………………………………………………………………14

Fig.1-4-1 SEM photographs of RF switch………………………………………………18

Fig.2-1Principle of operation of RF MEMS capacitive switch…………………………21

Fig.2-2 Pull-in phenomenon of RF MEMS switch………………………………………25

Fig.2-3 1-D dynamic model of RF MEMS switch………………………………………26

Fig.2-4 Stiction effect in DC-contact RF MEMS switch………………………………...29

Fig.2-5 Relationship between restoring force and actuated voltage…………………….30

Fig.2-6 Buckling of metallic membrane released with the power of 500W…………….31

Fig. 3-1 Center deflection vs actuation voltage for bowtie-like membrane…………….35

Fig.5-1 Schematic diagram of capacitive switch with elevated temperature……………48

Fig.5-2 Shifting of C-V curve……………………………………………………………49

Fig.5-3 Thermal stress of the membrane with an applied temperature of 27℃…………54

Fig.5-4 Thermal stress of the membrane with an applied temperature of 50℃…………54

Fig.5-5 Thermal stress of the membrane with an applied temperature of 100℃………..55

Fig.5-6 Thermal stress of the membrane with an applied temperature of 150℃………..55

Fig.5-7 Thermal stress of node 2395 vs temperature……………………………………56

Fig.5-8 Tensile stress of node 2395 vs Temperature……………………………………57

Fig.5-9 Finite element meshing of the membrane………………………………………59

Fig.5-10 The Von Mises stress of the membrane with the applied temperature of 50℃..59

Fig.5-11 The Von Mises stress of the membrane with the applied temperature of 150℃60

Fig.5-12 Shape of a fixed–fixed beam for different actuation voltages…………………61

Fig.5-13 C-V curve of RF MEMS switch………………………………………………62

Fig.5-14 Equivalent capacitance model of the switch…………………………………..63

Fig.5-15 Dewdrops on lotus leaf…………………………………………………………68

Fig.5-16 Corrugated profile of the dielectric layer………………………………………70

Fig.5-17 Semispherical profile of the dielectric layer…………………………………..72

Fig.5-18 Separation of the unit…………………………………………………………..73

Fig.5-19 Schematic of the discrete cubic unit……………………………………………74

Fig.5-20 SEM micrograph of FIB machining cylindroid array…………………………77

Fig.5-21 (a) the grey image used for NOVA200 to fabricate the nanostructure; (b) SEM of web-shaped rhombic array………………………………………………………………78

Fig.App Interpolation of desired values…………………………………………………84

Abstract

Along with the emergence of RF MEMS technology, integration of passive components with high Q value and functional components is now possible, providing an opportunity to attain full integration in a CMOS communication system. Among the components in RF MEMS devices, the switch is the critical unit that has the greatest effect on circuit performance. The RF switch is the frontend of the radio frequency circuit that is used for shifting between the signal channels. The MEMS-based switch employs microstructure to achieve the shifting between on-state and off-state. These switches possess very low insertion lose, high isolation, high linearity, miniscule power consumption, and high cut-off frequency. However, stiction caused by dielectric charging effects and humidity is one of the most common types of RF-MEMS failures, hindering the commercial application of RF-MEMS devices.

In this work, we employed ANSYS to simulate the development of compressive and tensile stress as a function of temperature, and obtained a relationship between the stress and the temperature. Based on this result, we can apply a temperature-stress curve to solve for the release voltage, and make predictions of the charge density at different temperatures.

Moreover, we also consider a modification of the dielectric layer geometry, and show that it's possible to obtain a beneficial reduction ratio using a different design of the dielectric layer's profile.

1 Introduction

1.1 Micro/Nanotechnology

According to Moore's law, with the same cost, the integration level would double per 18 months, and a new generation of products will come out per two to three years, as shown in Fig.1-1 [1, 2]. In the past 20 years, the development of the microelectronic techniques strictly follows Moore's law, the size of the devices has been reduced to submicron scale, and now research activities are focusing on nanometer scale. And it seems that this trend will last for the next 10 years. Thus, it asks for more advanced manufacturing techniques to satisfy the need of minimizing the electrical components. Among these advanced technologies, micro/nano technology possesses a critical position in promoting the development of the microelectronic industry. The requirement of the semiconductor or microelectronic industry in return accelerates the development of the micro/nano manufacturing technology.

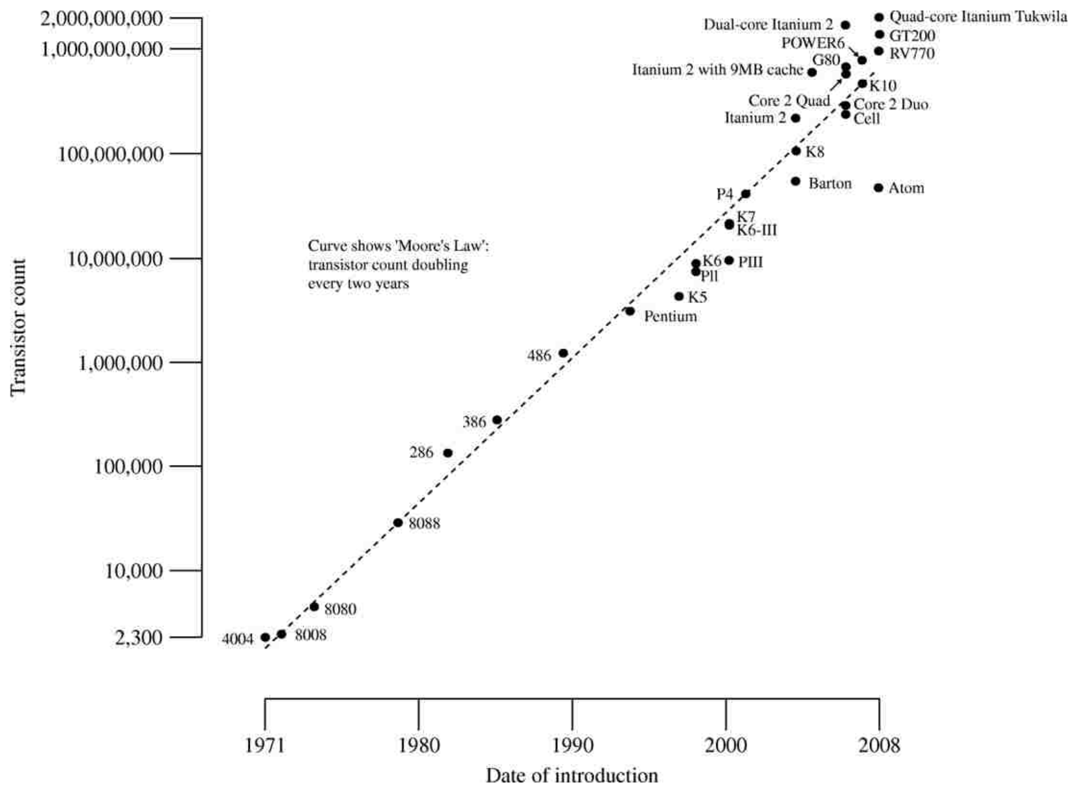

Fig.1-1 Moore's law and the counts of microdevices from 1971-2011

Micro/nano manufacturing technology is the general term for the preparing of the microstructures in micron or nanoscale. To date, there is no strict boundary between micro- and nanofabrication. Commonly, according to device size, manufacturing technologies can be categorized into three kinds, microfabrication refers to the preparing of the microstructures within the scale of $0.1\mu m$~100 μm, specifically, 0.1 μm~1 μm is the so-called submicron scale, the nanofabrication refers to the 1~100nm level fabrication. When the manufacturing scale is larger than 100 μm, it is attributed to the conventional precision fabrication technology.

Based on the methods and principles employed in the manufacturing process, micro/nanofabrication technology can be divided into the following categories:

material separation, material deformation, material adding, etc. In Section 1.1.1, we will outline some of the micro/nanofabrication techniques [3].

1.1.1 Category of Micro/Nanotechnology

Optical Lithography

Optical lithography, or called photolithography, was the first precision manufacturing technology employed in the semiconductor integrated circuits (ICs) industry. Since the very beginning of 1960s when the planar technology first came out, photolithography posses a major position in the fabrication of ICs, especially in VLSI manufacturing. Photolithography can achieve the projecting of series of 2-D patterns to the materials, and is capable of aligning the layers by each other precisely. Thus, we can prepare an IC structure with very complicated design [4].

Electron Beam Lithography

Electron beam lithography (EBL) uses the electron beam to directly expose the silicon with the photoresists deposited on it. This technique was developed from scanning electron microscope (SEM), which was created in 1965.

EBL system includes electron gun, electron lens, and electron deflector. Its resolution is mainly determined by the size of the beam and the scattering effect of the beam inside the photosensitive material. Generally speaking, the applied voltage used to accelerate the electrons is about 10~50kV, and the corresponding wavelength of the e-beam is about 0.1~0.05 $\dot{A}$. Therefore, it gives EBL a great

advantage in fabrication resolution, about 3~8nm. Moreover, the diffraction effect of the electron beam can also be ignored due to such short wavelength.

EBL can fabricate the desired pattern under the control of computer with short manufacturing cycle, and it is much easier to revise the figure we want to fabricate. Therefore, it is pervasively applied in the preparation of photo mask, and combining with specialized resist processes, EBL can attain the manufacturing of the structure with its size smaller than 10nm [4, 5].

Focused Ion Beam Technology

Focused ion beam (FIB) technology is basically the same with EBL. Both of them are achieved by apply a high voltage to focus the charged particles to a thin beam to fabricate the material. The different between FIB and EBL is that, FIB not only can be used as lithography, but also can fabricate the material directly. This unique characteristic is due to the fact that the mass of the ion is much bigger than electron, and the accelerated ions can sputter the material off directly. Compared with EBL, FIB possesses more advantages. As the mass of the ion is much heavier that electrode, the wavelength of the ion beam is much shorter than e-beam, and a much higher resolution as a result. Moreover, with heavier mass, the injection depth of the ion beam is lower than e-beam. Thus, it reduces the scattering effect and makes the energy of the injected ions much easier to be absorbed by the materials [4, 6].

Etching Technology

Etching technology is using physical or chemical methods to remove the unprotected parts from the surface of the material. Etching technology includes wet etching, e.g., chemical wet etching, and physical dry etching, e.g., plasma dry etching. With a certain etching rate, the etching depth is the function of time. And the etching rate is also affected by many factors [4]. The etching rate of wet etching will be various with different crystal orientations. On the contrary, the etching rate of dry etching has no correlation with the crystal orientation, but is determined by the directions of the wafer. If the etching rate is crystal dependent, the etching process is anisotropic. If the etching rates are identical in all direction, it is called isotropic [7].

1.2 Brief Introduction to MEMS

With the development of micro/nanofabrication technology, in 1980s, another technical revolution, which is called microsystem technology, gradually emerged and came to our lives. Microsystem, which also called Microelectromechanical system (MEMS), is the system that integrated with microstructures, microsensors, microactuators, power sources, etc., ranges from $1\mu m{\sim}1cm$. Combined with these components, MEMS devices are capable of achieving so many functions, like sensing, actuation, wireless communication, energy transfer and data processing, which makes the chips no longer subjected to the signal processing only. And generally, we can attain the fabrication of microsystem by employing the Integrated Circuit manufacturing technology and microfabrication technology. MEMS devices hold many advantages, e.g., miniaturized size in microscale, integrated with multi-

functional components, low-cost, high stability, mass-produce, low power consumption, inactively addressing, and so forth. It has already been applied in measurement, wireless communication, energy, biomedicine, military affairs and national defense, aviation, automotive electronic and consumer electronic fields, and so forth [8].

Microsystem is more often referred to a device with relative comprehensive functions. However, due to some restrictions of manufacturing techniques, many microsystems only contain several kinds of functional components. Under such circumstances, we prefer using MEMS instead of microsystem.

1.2.1 Category of MEMS

Most MEMS devices contain microsensors and microactuators, which can be attributed to transducers. Some other applications of MEMS devices are inactively addressing and controlling. Equipped with corresponding functional components, MEMS device can be applied in specific fields, like temperature or pressure sensing, torque and force output, wireless communication, clinical measurement, and so on. The applications of MEMS in these fields correspondingly generate many branches of MEMS, like RF MEMS, BioMEMS, Optical MEMS, etc.

Microsensors fall into two categories, i.e., physical and chemical [7], and they are used to sense and measure the physical or chemical information from the environment. Microsensor has the longest history, earliest industrialization, and highest production. Fig. 1-2-1 shows the micro-acceleration sensor ADXL202,

developed by Analog Devices (ADI). Figure (a) to (c) are the chip, packaging image, static state of acceleration sensing unit, and measuring state of acceleration sensing unit, respectively. When acceleration is applied, the inertia force will change the space between the interdigitated fingers, and this will result in the variation of the capacitance, and the voltage on the capacitors as well. Thus, this changing of the voltage will feedback to the control system, and after the processing of this signal, the exact acceleration will be output [8].

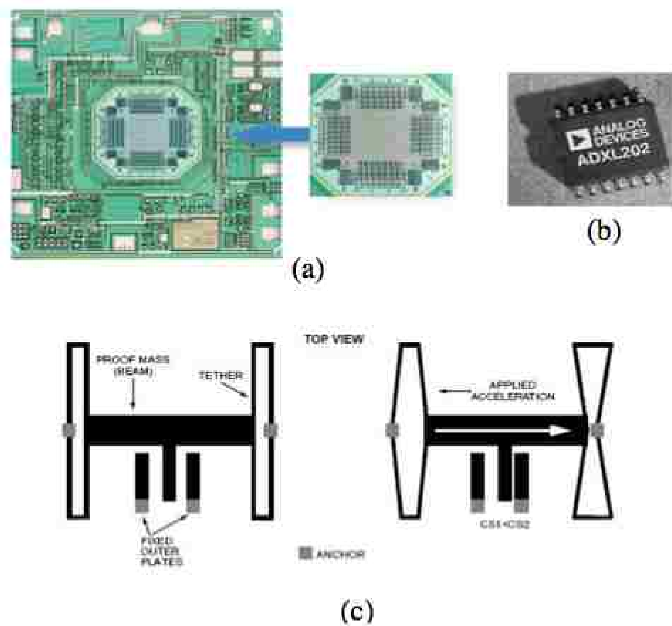

Fig.1-2-1 ADXL202 micro-acceleration sensor. (a) chip; (b) packaging image; (c) static state and measuring state of acceleration sensing unit

Generally, microactuator is used to transform the energy from nonmechanical (e.g. electric domain, magnetic domain, etc.) domains into mechanical domain. It is another important component of MEMS device. Fig. 1-2-2 shows the micro-electrostatic motor with the diameter of 100μm, developed by University of

California, Berkeley [8]. When we apply different bias on the different electrodes, this microactuator will output the rotation due to the electrostatic force. The microactuator also has many other actuation methods, like thermal expansion, electrochemical reaction, magnetostriction, piezoelectric effect, etc.

Fig.1-2-2 micro-electrostatic motor

RF MEMS is a significant application of MEMS technology in wireless communication area. With integrating of switch, resonator, phase shifter, varactor, tunable oscillator, filter, and some subsystems together, RF MEMS devices can greatly improve the reliability and signal processing ability, reduce the cost and size of the wireless communication system. More details will be discussed in section 1.3 and 1.4.

Biomedical MEMS (BioMEMS) and lab on a chip (LOC) is another research hotspot in MEMS area. It includes the investigation of drug releasing, clinical measurement and diagnosis, clinical supervision, tumor cell detection and clearance,

biochemical analysis, etc. LOC can integrate multiple functional units into a single chip, and it can achieve many functions, like drug delivery, separation, mixture, purification of the biological samples, and cell detection, to name a few. With the help of BioMEMS and LOC, we can easily control the dosage of the medicine, reduce the surgery pain, decrease the side effect of the drug, etc.

1.2.2 Characteristics of MEMS

The design, fabrication, and application of MEMS involve multiple fields of science and engineering, e.g., electronics, mechanics, physics, chemistry, biology, fabrication technology, optics, material, energy, civil and environment engineering, etc., which make MEMS a multidisciplinary cut-off technology [4, 7, 8].

(1) **Tiny size.** Generally speaking, the length scale of MEMS device ranges from micron to millimeter. With such small dimension, MEMS devices possess many advantages over conventional devices, like high resonance frequency, thermal mass, higher power density, and low soft springs [7]. However, miniaturizing of the system may not always bring us benefits. For example, when we fabricating a cantilever beam, the spring constant will decrease with the decreasing of the dimension. Furthermore, the relative dimension error of the MEMS device is much bigger than normal mechanical devices. For instance, the relative accuracy of traditional macroscopical mechanical device can reach to 1:200000, on the contrary, MEMS only has its accuracy with about 1:100.

In microscopic world, some factors that related to surface area (e.g. surface tension) become the major factors, and these devices are strictly subjected to the scaling law. To this end, MEMS can be attributed to surface science.

(2) **Monolithic Integration.** One of the most significant characteristics of MEMS is that, it can integrate sensors, actuators, and some subsystems together with electronic components on a single chip. This monolithic integration format can tremendously improve the signal quality, reduce the system noise, shorten the signal transmission time, etc.

(3) **Multi-energy domain system.** As we mentioned before, MEMS technology includes the energy transformation between multiple domains. This characteristic makes MEMS devices the capability of working in many different fields, and it become the bridge to connect these fields together.

(4) **Based on microfabrication technology.** MEMS is originated from IC technology, and due to its tiny size, it inevitably involves many microfabrication techniques during the manufacturing process, like lithography, CVD, EBL, RIE, etc. Moreover, as MEMS devices are not merely subjected to the electronic field, the Integrated Circuit manufacturing technology will no longer satisfies the requirement of MEMS manufacturing. More and more advanced technologies should be involved to achieve the fabrication of MEMS devices in specific fields.

1.2.3 Present Situation of MEMS industry

The market needs and the development of microfabrication technology directly lead to blooming of MEMS industry. Till now, the commercialization of MEMS products receives an unprecedented success, like pressure sensor, microcontroller (MCU), accelerometer, acceleration sensor, gyro, microfluidic chip, microphone, ink-jet printer nozzle, DMD, etc. Furthermore, RF MEMS, BioMEMS and LOC, optical MEMS and power MEMS also present huge market potential as well. There are about 250 companies and organizations engaging in MEMS investigation and development, and most of these companies are distributed over the US, Europe, Japan, Taiwan, and some other countries and regions. In 2005, the top 15 MEMS manufacturers are: TI, HP, Bosch, Lexmark, ST, Epson, BEI, Canon, Freescale, Denso, ADI, GE-Novasensor, Omron, Honeywell, and Delco. The top 20 MEMS manufacturers occupy 87% MEMS market share worldwide [4, 8].

1.3 RF MEMS Technology

MEMS technology has contributed to the development of many fields. There is one application of MEMS technology worthy to be noted, it is named RF MEMS. From its name, we can see that it is an application of MEMS in radio frequency area. In wireless communication, the new generation of communication devices, like smartphone and Bluetooth, are looking for the smaller circuits with much lighter weight. On the other hand, satellite communication and radar detection require much faster data processing speed, higher reliability and isolation, and lower insertion loss and power consumption. The emerging of RF MEMS technology perfectly meets

these demands, which gives RF MEMS a very promising potential in wireless communication area.

Early investigation of RF devices started in the end of 70s [9], and mainly focused on the pressure sensor, temperature sensor, accelerometer, etc. However, most of the devices still remained at the experimental stage. After a series researches of RF MEMS switches and varactors in military radar area conducted by Hughes Research Labs, Rockwell Science Center, and Texas Instruments (Rathon), which were sponsored by DARPA in the beginning of 1990s, RF MEMS got its real debut to the world. All these immense potential of RF MEMS in defense and commercial areas, abstract more and more attentions in this field, which in turn accelerate its development worldwide.

1.3.1 Configuration of RF MEMS

Basically, RF MEMS devices can be classified into two parts, stationary unit and movable unit. The stationary unit includes transmission line, static fixed-value inductor, filter, etc., while the movable unit includes RF switch, resonator and varactor and the phase shifter that consists of switches and varactors. As the critical component in RF MEMS device, RF switch consists of two parts, i.e., mechanical part and electrical part [10]. Electrostatic, electromagnetic, or some other methods are employed in actuating the mechanical movement of the RF switches. For electrical part, the RF switch can be configured with series or shunt connection. The contact type can be either ohmic contact or capacitive contact. These various

contact types, circuit implementations, and actuation methods give us plenty of options.

1.3.2 RF MEMS Advantages

(1) **Performance improving and size decreasing.** An RF MEMS device is two orders of magnitude smaller than conventional wireless communication device. Thus, using RF MEMS devices to substitute for the isolated components in wireless communication system can tremendously reduce the dimension and weight of the integrated system, as shown in Fig. 1-3-1 [11]. Moreover, due to their small size, low power consumption, high Q value, and high reliability, RF MEMS devices can be immensely integrated in wireless communication systems, and with different combination of these functional modules, we can develop more novel functions and applications [8].

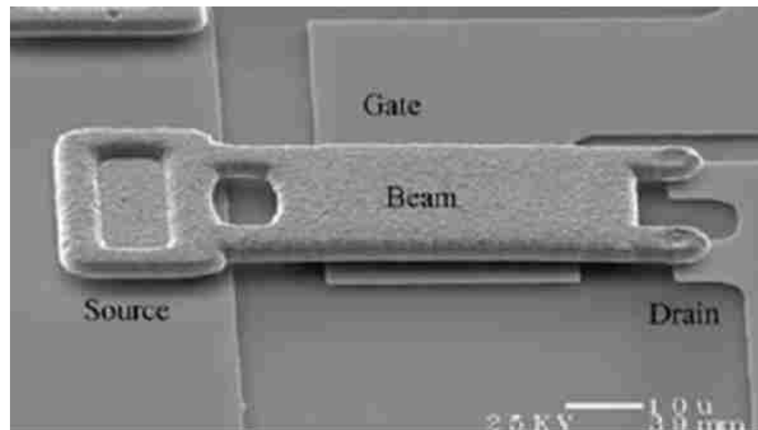

Fig.1-3-1 Scanning electron microscope photograph of a MEMS switch, showing the source, gate and drain

(2) **Complete integrated system**. Most RF MEMS devices` manufacturing processes are compatible with ICs technology, which make them capable of achieving system-on-a-chip (SOC), which in turn further improve the performance of communication system, and make the whole system more integrate. It can simplify the processes of manufacturing and packaging, and greatly reduce the cost as well [8].

(3) **Reducing the power consumption**. Generally, the RF switches are actuated by electrostatic force, and the actuation voltage is relatively low, which reduce the direct currents in the circuits. And the small size and weight of the devices also decrease the required actuation power. Moreover, as the isolation and insertion loss performance of RF switches are much better than FETs and PIN transistors, even being immensely integrated in wireless communication system, it will still maintain the power consumption of the system within a relatively low level.

1.4 RF MEMS Switch

As the overarching component of RF MEMS devices, RF switches have a great potential in microwave monolithic integrated circuits (MMICs). The switch is the front-end component used in switching the signals between the channels. To date, most RF circuits integrate FET and PIN transistors as the switches. However, the isolation of FET cannot satisfy the requirement of modern RF device, and the power consumption of PIN transistor is very high. Moreover, the cost of integrating these two components with CMOS is relatively high. By contrast, RF MEMS switch possess many advantages over FET and PIN transistors, such as high isolation when

open, low insertion loss when closed, low power consumption, high cutoff frequency, high linearity, etc. The comparison of RF MEMS switch, FET and PIN transistor are shown in Table.1-1.

Table.1-1 Performance comparison of RF MEMS switch, FET and PIN transistor [10]

Parameter	RF MEMS	PIN	FET
Voltage (V)	20-80	$\pm 3-5$	3-5
Current (mA)	0	3-20	0
Power consumption (mW)	0.05-0.1	5-100	0.05-0.1
Switching time	1-300μs	1-100ns	1-100ns
C_{up} (series) (fF)	1-6	40-80	70-140
R_s (series) (W)	0.5-2	2-4	4-6
Capacitance ratio	40-500	10	n/a
Cutoff frequency (THz)	20-80	1-4	0.5-2
Isolation (1–10 GHz)	Very high	High	Medium
Isolation (10–40 GHz)	Very high	Medium	Low
Isolation (60–100 GHz)	High	Medium	None
Loss (1–100 GHz) (dB)	0.05-0.2	0.3-1.2	0.4-2.5

Power handling (W)	<1	<10	<10
Third-order intercept point (dBm)	+66-80	+27-45	+27-45

All these features make RF switches widely used in radar, satellite communication, wireless communication, etc [12].

There are several methods to actuate the switch, including electrothermal [13], magnetostatic [14], and electromagnetic actuation [15, 16, 17]. Among these various actuation mechanisms, electrostatic actuation [18, 19, 20] is widely accepted by researchers and manufacturers. Electrostatic actuation possess many advantages, such as low power consumptions and simple manufacturing process. However, the main drawback of electrostatic actuation is its high actuation voltage, and the mechanical stability is relatively low as well [8]. Fig.1-4-1 shows the electrostatic actuation of RF MEMS switch.

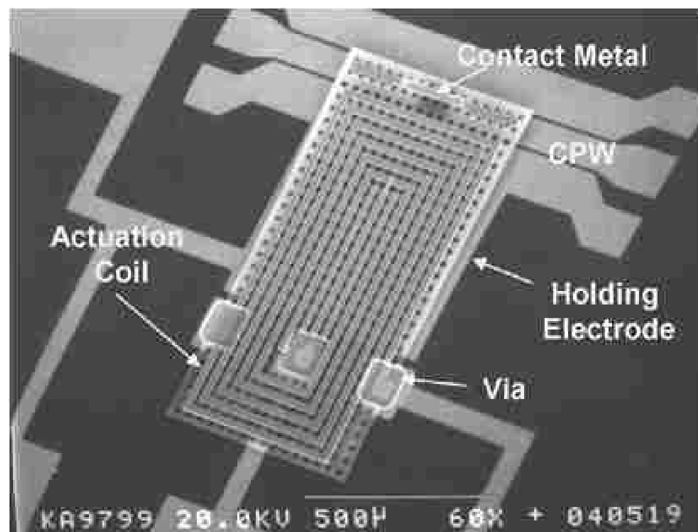

(a)

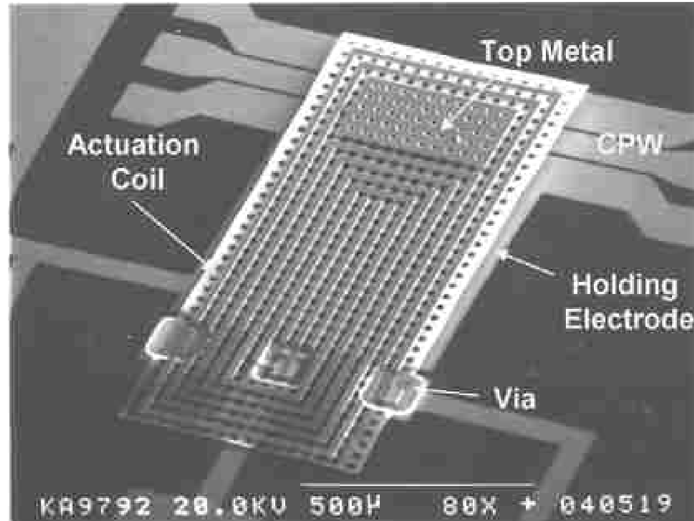

(b)

Fig.1-4-1 SEM photographs of RF switch. (a) Series connection. (b) Shunt connection [21]

Based on the contact behavior, RF switches can be categorized into two kinds, ohmic contact switches [22] and capacitive switches [23]. The ohmic contact switch achieves the signal input and output by the controlling of metal-metal contacting, and it is applicable for low and high frequency. For capacitive switches, there is a dielectric layer deposited on the transmission line, which is used to prevent direct contact of the metallic membrane with the bottom electrode. By controlling the actuation voltage, the displacement between the membrane and the bottom electrode can be changed, thus achieving switching between on-state and off-state.

Failure Mechanisms of RF MEMS Switches

There are many phenomena that will cause the failure of the RF MEMS switch, including fracture, creep, delamination, electromigration, thermal effect, degradation

of dielectric, stiction, wear, etc. Here, we mainly give a brief introduction of stiction and thermal effects [24].

Stiction. When we apply an actuated voltage between the membrane and the bottom electrode, the membrane will deflect downwards, and contact with the dielectric layer. However, when the switch operates for a certain period of time, the accumulation of charge in the metallic membrane and the dielectric layer will reach a certain level, which in turn can generate an additional "pull-in" force on the switch, and the switch will no longer spring back, even after we remove the actuated voltage. In such circumstances, the switch is said to be stuck, and we call this phenomena stiction [25, 26, 27]. To date, there is neither an effective model to predict the dielectric charging behavior accurately, nor an effective solution to diminish the dielectric charging effect.

Due to the small size of the structure, the moisture of the air, and the molecular Van der Waals force may aggravate the stiction failure [28]. For a larger scale macrostructure, the capillary forces that arise from high environment humidity, and the Van der Waals forces between molecules are ignored. However, for RF MEMS switches, the membrane is very light, which results in a low restoring force when compared with the macrostructure, so the surface forces should be taken into account.

Temperature issues. It has been reported that, elevating the ambient temperature of the RF MEMS switch can lead to buckling of the RF switch, which can cause permanent failure of the RF MEMS device. On the other hand, decreasing the temperature can lead to an increase in the pull-in voltage, which is also an undesirable situation, as a large pull-in voltage will add additional power consumption to the

whole system, and significantly reduce the life of the RF switch [29, 30]. More details will be discussed in Chapter 3.

1.5 Structure of Thesis

This thesis is arranged as follows. Chapter 2 provides a basic description of mechanical model of RF MEMS switches. Chapter 3 mainly discusses the thermal effects on RF MEMS switches, and tries to find some solutions to deal with it. In Chapter 4, a background of thermoelasticity is provided, which will be used in the following study of RF switches. For Chapter 5, we employ ANSYS to simulate the thermal effect and find out the relationship between temperature and stresses. We also applied these results to solve for the charge density and the release voltage, which are the critical characteristics in an RF switch. Furthermore, we discuss the effect of the dielectric layer geometry on the stiction failure, and obtain a reduction ratio with different designs of the dielectric layer profile. In Chapter 6, we draw conclusions based on the results we obtained in the previous chapters, and pose some questions that still need to be solved as well.

2 Basic Mechanical Behavior of RF MEMS Switches

2.1 Mechanical Model of Electrostatic Actuation RF MEMS Switches

As discussed in Section 1.4, electrostatic force is generally applied in actuating the RF MEMS switch. By changing the distance between membrane/cantilever and transmission line, the RF circuit can be easily switched between its on- and off-state.

2.1.1 Static State Mechanical Characteristics of Electrostatic Actuation RF MEMS Capacitive Switch

Fig.2-1shows the structure of electrostatic actuation RF MEMS shunt switch. The dielectric layer is about 0.2~2 μm thick, and it is used for isolating the DC when the switch is at its on-state.

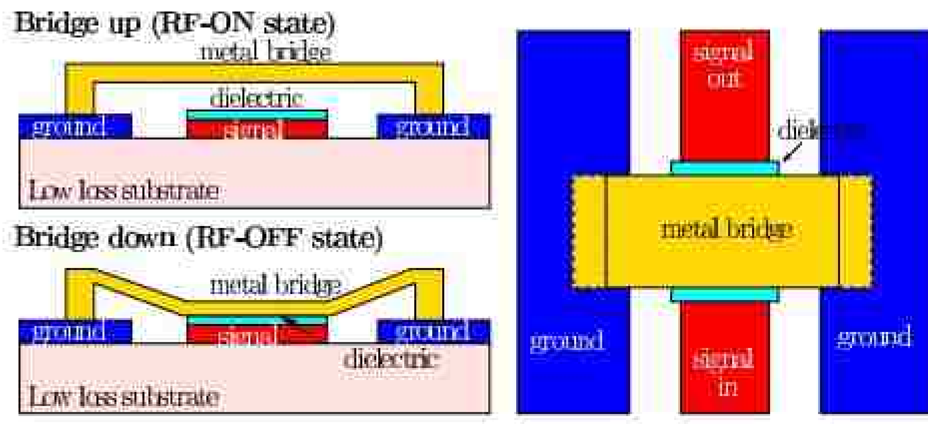

Fig.2-1Principle of operation of RF MEMS capacitive switch [31]

Based on this configuration, we plan to solve for the most significant parameter in RF MEMS switch, the pull-in voltage.

For the RF capacitive switch, the metallic membrane and bottom electrode together constitute a capacitor. Considering the thickness of the dielectric layer, we assume that the widths of the membrane and bottom electrode are w and W, respectively, the capacitance of the RF switch is [10]:

$$C = \frac{\varepsilon_0 A}{d} = \frac{\varepsilon_0 A}{g(x,t) + \frac{t_d}{\varepsilon_r}} = \frac{\varepsilon_0 wW}{g(x,t) + \frac{t_d}{\varepsilon_r}} \quad (2.1)$$

where t_d , ε_0 and ε_r are thickness, permittivity of air, and relative dielectric constant of the dielectric layer, respectively, and $g(x,t)$ is the distance between the upper and bottom electrodes, and it is the function of time and the position on the membrane. Thus, we can easily find out the capacitance in the on-state and off-state, i.e., $C_{on} = \frac{\varepsilon_0 A}{g_0 + {t_d}/{\varepsilon_r}}$, and $C_{off} = \frac{\varepsilon_0 \varepsilon_r A}{t_d}$.

When applying an actuation voltage between two parallel plates, the corresponding electrostatic force inside the plates equals the gradient of the electric energy U with respect to the vertical displacement between the upper and bottom electrodes [7].

$$F_e = \left|\frac{\partial U}{\partial x}\right| = \left|\frac{1}{2}\frac{\partial C}{\partial g}V^2\right| = \frac{1}{2}\frac{\varepsilon_0 wWV^2}{(g + \frac{t_d}{\varepsilon_r})^2} \quad (2.2)$$

When the electrostatic force equals the restoring force of the upper electrode (membrane or cantilever beam), we have

$$F_e = \frac{1}{2}\frac{\varepsilon_0 wWV^2}{(g + \frac{t_d}{\varepsilon_r})^2} = F_k = k(g_0 - g) \quad (2.3)$$

Taking the capacitance reduction caused by the dielectric layer roughness into account, the equation above should be rewritten as [10]

$$F_e = \frac{1}{2}\frac{\varepsilon_0 \varepsilon w W V^2}{\left(g + \frac{t_d}{\varepsilon_r}\right)^2} = F_k = k(g_0 - g) \tag{2.4}$$

$$\varepsilon = \begin{cases} 1 & g \neq 0 \\ 0.4\sim0.8 & g = 0 \end{cases}$$

More details about the geometry of dielectric layer will be discussed in section 5.3.

In such a circumstance, if we keep increasing the actuation voltage, the upper electrode will be pulled downwards gradually, as a result of the increasing electrostatic force. According to Equation (2.4), we can obtain the expression for actuation voltage as a function of displacement g.

$$V = \sqrt{\frac{2k}{\varepsilon_0 \varepsilon w W}(g_0 - g)(g + \frac{t_d}{\varepsilon_r})^2} \tag{2.5}$$

where g_0 and k are the original displacement between two plates and the spring constant, respectively.

When the voltage reaches a certain value, the membrane displaces rapidly and fully contacts with the dielectric layer. This critical voltage will satisfy the following equation,

$$\frac{\partial V}{\partial g} = \frac{\partial}{\partial g}\sqrt{\frac{2k}{\varepsilon_0 w W}(g_0 - g)(g + \frac{t_d}{\varepsilon_r})^2} = 0 \tag{2.6}$$

Solving this equation, we can obtain the critical position $g = 2/3g_0$, and $g = g_0$ (trivial solution), which predicts the snapping down position of the membrane.

Substituting this critical position $g = 2/3g_0$ into Equation (2.5), we can derive the pull-in voltage

$$V_{pull-in} = \sqrt{\frac{2k}{3\varepsilon_0 wW} g_0 (\frac{2}{3} g_0 + \frac{t_d}{\varepsilon_r})^2} \tag{2.7}$$

Fig.2-2 shows the pull-in phenomenon of RF MEMS switch. From this figure, we can see that the biggest actuation voltage occurs at $g = 1/3g_0$, it matches the result we obtained before. And after this position, the membrane suddenly snaps down onto the dielectric layer, as shown with the dashed line. It indicates that, when the membrane is at the critical position $g = 1/3g_0$, the system is in an unstable state. Once the actuation voltage exceeds this value, the membrane will rapidly contact the transmission line, and the switch is in its on-state, and the signal will be coupled to the ground. This is called the pull-in phenomenon, and the actuation voltage at this time is called the pull-in voltage, which is the critical parameter pervasively used in estimating the power consumption of the system.

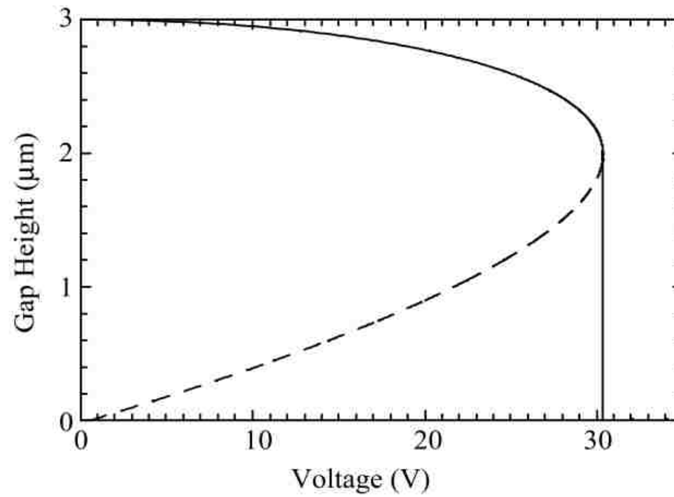

Fig.2-2 Pull-in phenomenon of RF MEMS switch [10]

2.1.2 Dynamic Analysis of the Mechanical Characteristics of Electrostatic Actuation RF MEMS Switch

In the last section, we obtained a significant parameter for the RF MEMS device. Furthermore, by analysis of frequency response of fixed-fixed beam or cantilever beam switches, we can obtain more useful parameters, such as switching time, the mechanical bandwidth, and the effect of thermal noise. The 1-D RF MEMS switch, model including the damping effect, is shown in Fig.2-3.

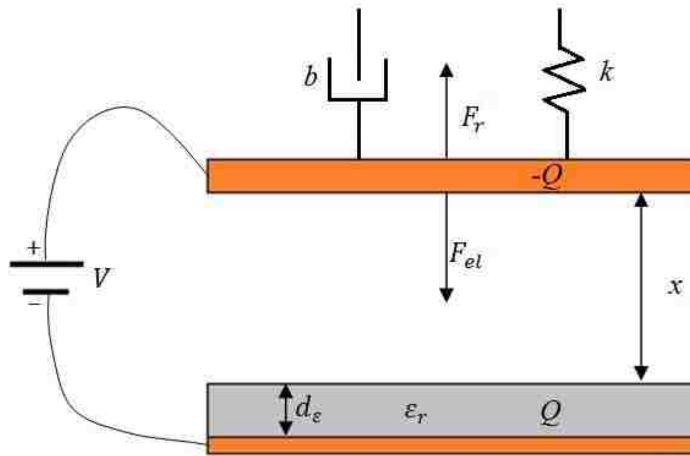

Fig.2-3 1-D dynamic model of RF MEMS switch

The dynamic response is given by d'Alembert's principle, the governing equation of the movable beam behavior is [10, 32]

$$m\frac{d^2x}{dt^2} + b\frac{dx}{dt} + kx = F_{ext} \tag{2.8}$$

where m is the mass of the movable beam, b is the damping coefficient, F_{ext} is the external force exerted on the membrane, x is the deflection of the upper plate. It should be noted here that the mass m is the effective mass of the membrane, and it is about 0.35~0.4 times of the actual membrane mass. It is determined by the size of the bottom electrode, spring constant and thickness of the membrane [10, 33].

By taking the Laplace transform, Equation (2.8) can be written as [10]

$$\frac{X(j\omega)}{F(j\omega)} = \frac{1}{k}\frac{1}{1-({}^{\omega}/{}_{\omega_0})^2 + {}^{j\omega}/{}_{(Q\omega_0)}} \tag{2.9}$$

Here, $\omega_0 = \sqrt{k/m}$, which is called resonant frequency, and $Q = {k}/{(\omega_0 b)}$ is the quality factor of the switch, which is an important characteristic parameter used to evaluate the switch performance [10]. There are two kinds of air damping involved in the microsystem, squeeze film damping and slide film damping. Imaging that, there are two parallel placed plates, if one plate moves longitudinally with respect to the other one, the air between the plates will hinder the movement of the plate due to the viscous force of the air, and this is called slide film damping. Squeeze film damping is the kind of air damping that parallel plates experience due to the changing of the spacing inside the capacitor, caused by the vertical movement of the plates. Apparently, the damping of RF MEMS switches belongs to the squeeze film damping category.

The air model of the RF MEMS switch can be analyzed by the viscous hydrodynamics theorem. And an important nondimentional squeeze number σ can be expressed as [10, 34, 35].

$$\sigma = \frac{12\mu_e l^2}{P_a g^2}\omega \tag{2.10}$$

In this equation, μ_e stands for air viscosity, P_a is the pressure, ω is the applied mechanical frequency, l is the characteristic length of the rectangular plate, g is the distance between two parallel plates.

Equation (2.10) is derived based on a parallel plate model with no holes in it. However, for the sake of reducing the elastic modulus and releasing the residual stress (this will be discussed in Section 3.2), most of the current design of the RF

switch, which will contain a certain amount of holes, and the air between the plates will no longer only escape from the sides. For this reason, the squeeze film damping is not that important, and sometimes can be ignored during design [10].

2.2 Failure Phenomenon of RF MEMS Switches

A well operated RF MEMS switch is expected to work for more than billions cycles, and it has been reported that by carefully preparation and material selection, the lifetimes of RF switch can be up to 250 billion operation cycles or even more [36, 37]. However, normal RF switches are still far behind this target. As mentioned in Section 1.4, there are several factors that affect the performance of an RF switch. Among them, stiction failure and buckling failure are two overarching failure mechanisms of RF MEMS switch, and greatly affect the reliability of RF switches.

2.2.1 Stiction Effect in DC-Contact MEMS Switch

As we talked about before, the stiction effect is a significant failure phenomenon in the operation of RF MEMS switch, shown in Fig.2-5. Humidity and charging are two major effects that will result in stiction failure of the RF switch. A moist environment will lead to stiction because of capillary forces, and surface charging is also expected to be sensitive to ambient atmospheric environment [38], which may increase the electrostatic force of the capacitor. Both these two factors will greatly hinder the performance of the RF switch.

With the operation of the RF MEMS switch, the accumulation of the bulk charges and surface charges will enhance the electrostatic force, which becomes another

reason for stiction failure. However, there is still no effective theory that perfectly describes the charging behavior in the switch. More effort needs to be put in this area to obtain an accurate model to deal with this issue.

Fig.2-4 presents the principle of the stiction effect in DC-contact RF MEMS switch. Once stiction occurs, the sticking force is bigger than the restoring force, and the switch is unable to open again.

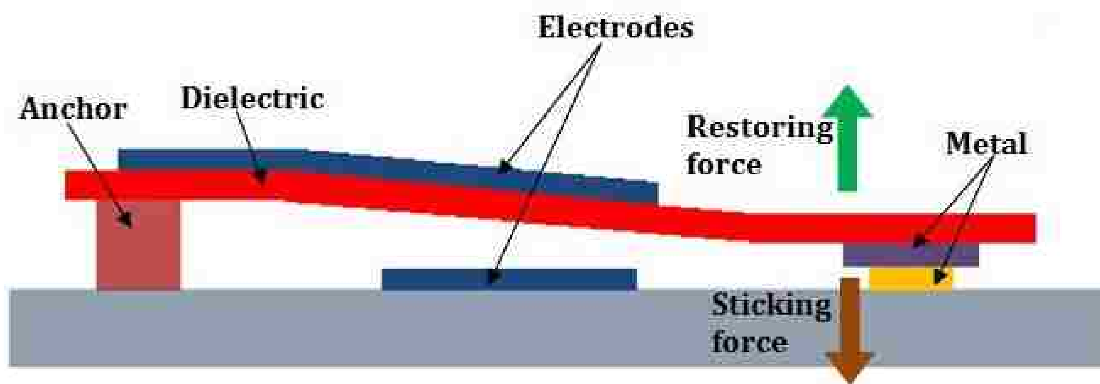

Fig.2-4 Stiction effect in DC-contact RF MEMS switch

In order to reopen the switch, we need to increase the applied voltage to overcome the stiction force. Fig.2-5 shows the relationship between the elastic restoring force and applied voltage [39]. With an increase in the applied voltage, the beam bends towards the bottom electrode gradually, which in turn increases deformation of the beam, resulting in a quadratically increasing elastic restoring force. Once the restoring force is equal to the stiction force, the membrane can spring back to its original position, and at this time, the applied voltage is far beyond the pull-in voltage.

From Fig.2-5, we can see that the required actuation voltage for the necessary restoring force is quite large (approximately 80V). However, this high actuation voltage will definitely increase the power consumption, and may bring more thermal effects to the system, which will damage the device reliability.

In order to increase the restoring force, we can increase the spring constant first. The spring constant of the cantilever beam can be described as [7]:

$$k = \frac{F}{x} = \frac{3EI}{l^3} = \frac{Ew}{4}\left(\frac{t}{l}\right)^3 \tag{2.11}$$

Therefore, we can increase the thickness or reduce the length of the cantilever beam, or introduce more residual stress, to increase the spring constant, so that we can obtain a larger restoring force. However, the pull-in voltage will also increase as a result.

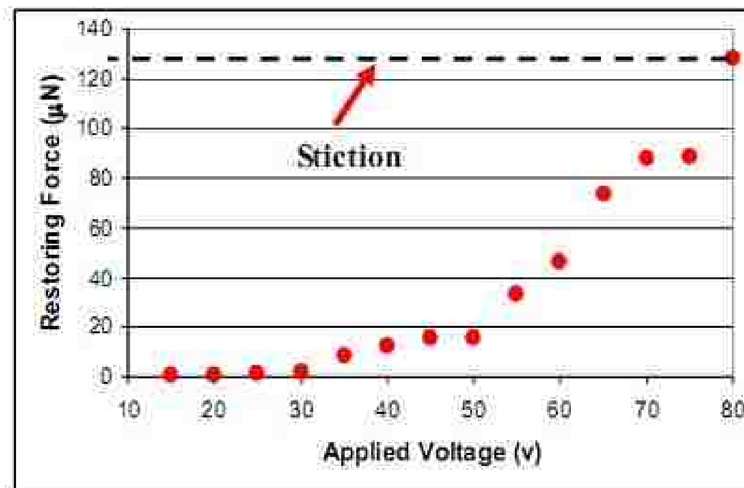

Fig.2-5 Relationship between restoring force and applied voltage [39]

2.2.2 Buckling Deformation Effect in DC-Contact MEMS Switch

Buckling refers to the sudden change in material's equilibrium configuration. When the loads on the structure reach a certain value, if we add a small increment in load to the structure, the equilibrium configuration will suddenly change. In RF MEMS switches, buckling failure is often considered to be a substantial out-of-plane deformation of the membrane, which arises from excessive compressive in-plane stress. Commonly, a high temperature working environment may easily result in a large compressive stress in the switch, and this may lead to the buckling failure. There are several kinds of buckling behavior observed in the practical working of RF switches, including bubble buckling, telephone cord buckling, and straight sided buckling. Fig.2-6 shows the buckling of the metallic membrane of an RF MEMS switch.

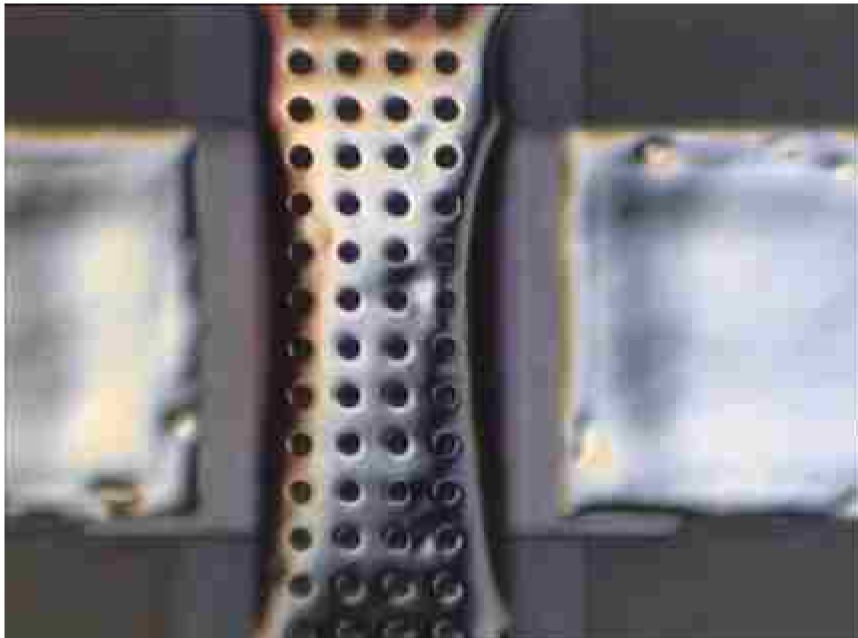

Fig.2-6 Buckling of metallic membrane released with the power of 500W [40]

Consequently, the buckling effect is a significant failure phenomenon in DC-contact RF MEMS switch. How to prevent structural failure from buckling deformation is an important topic in the study of reliability of RF MEMS switches. More details will be discussed in Section 3.2.

3 Thermal Effects on Switches Reliability

As discussed in Section 1.4, temperature has a considerable effect on RF MEMS switch reliability. However, in many cases, RF MEMS switches have to work under a very high or low temperature environment. For instance, during the packaging process, these tiny components will be subjected to a relative high temperature, e.g., 150℃ or even higher [41]. On the other hand, for practical applications in aircraft condition monitoring and satellite communication, RF MEMS switches are commonly subjected to a working environment with a really low temperature, e.g., below -50℃ [42]. As indicated in Ref.[30], an elevated temperature will result in membrane buckling, which may further cause the premature failure of the device. This phenomenon is undesirable in many practical applications. By contrast, a much lower environment temperature will increase the pull-in voltage, which could compromise the reliability and lifetime of the switch due to the dielectric charging effect [43]. Moreover, a reduction of actuation voltage by 6V will lead to a ten times improvement in the longevity of capacitive RF switch [30, 43, 44]. Therefore, how to understand the thermal effects on RF MEMS switches and construct a model to predict the reliability of switches under low or high temperature presents a great challenge for researchers in the study of RF MEMS switches.

3.1 Low Temperature Effects on RF MEMS Switches

The major aspects usually of the greatest concern to electrical engineers are isolation and insertion of RF MEMS switches, while power consumption and reliability of the devices

are the two main parameters that are related to mechanical engineering. As is the major failure mechanism in RF MEMS switches operation, the stiction effect seriously influences the reliability of an RF MEMS switch. To date, there are still some questions that need to be further studied regarding stiction phenomenon. However, numerous research results provide us with an empirical conclusion, with an increase in the pull-in voltage, the accumulation of electrons can become severe, which will lead to premature switch failure.

As mentioned before, a low environmental temperature will lead to an elevated pull-in voltage. Prof. Espinosa`s group has conducted much valuable research in this direction [30, 43]. In his research on the effect of temperature on capacitive RF MEMS switches, he discovered that, when the temperature varied from -40°C to 50°C, the actuation voltage decreased from 120V to ~16V correspondingly. Fig.3-1 shows the relationship between applied voltage and center deflection under temperatures from -40°C to room temperature [43].

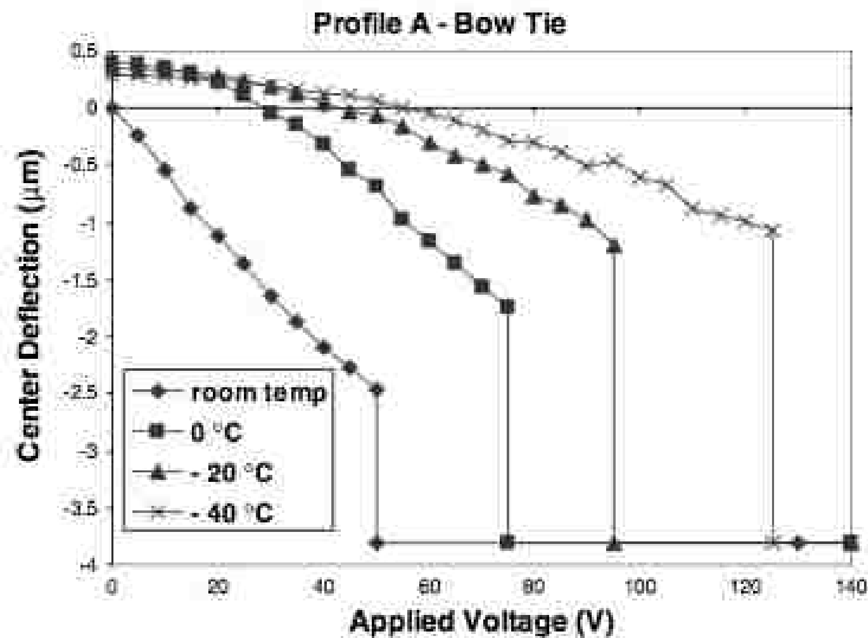

Fig. 3-1 Center deflection vs actuation voltage for bowtie-like membrane

3.2 High Temperature Effects on RF MEMS Switches

Due to the mismatch in materials thermal expansion coefficients (TCE), the interaction between the components of the switch will generate thermal stresses within the device. Moreover, when the temperature rises, these thermal stresses can lead to a premature buckling of the membrane, which in turn will cause failure of the devices. However, by an elaborate design of out-of-plane profile and optimizing of fabrication process, this premature buckling failure can be effectively diminished [45].

During the packaging or microfabrication process of RF MEMS devices, the switches will be subjected to a high temperature environment, which is usually 100℃ or above.

Meanwhile, the dissipation of the power during the cycling of the device increases the temperature of the components as well. Both of these two factors will equally contribute to the variations in temperatures, and as a result compromise the reliability of the switch. In order to maintain a pull-in voltage within an acceptable range, we should identify a structure and material of the switch that is insensitive to the change of temperature [46].

As the buckling temperature is a function of manufacturing residual stress state, out-of-plane geometry of the switch, and mismatch between material TCEs [43], there are several strategies to minimize the buckling failure: adding additional holes on the membrane, revising the out-of-plane profile of the membrane, controlling the residual stress state within a beneficial range, and specifying materials with similar TCEs.

Holes on membrane. The existence of the holes in the metallic membrane can favorably modify the residual stress, and reduce the equivalent elastic modulus as well. Here, the residual stress is reduced to about $\sigma = (1 - \mu)\sigma_0$, where μ is the ratio of the remaining link width to the pattern pitch, and σ_0 denotes the residual stress of the original membrane, when there is no holes in it. Moreover, these existing holes can reduce the mass of the membrane, which in turn improve the mechanical resonant frequency of the membrane. However, the existence of the holes may also reduce the capacitance of the switch in its "DOWN" state, and this should be taken into account when we design the structure [10].

Out-of-plane profile. The out-of-plane geometry of the membrane is also a significant design variable. By specifically designing the out-of-plane profile, the membrane can be made more compliant [43, 47]. In other words, we could make the switch very sensitive

or insensitive to changes in the environment temperature by using different kinds of geometric design. Moreover, by effective design of the out-of-plane geometry, we can successfully control the stress state inside the beam, while manipulating the actuation voltage within an acceptable range as well. To date, there are no effective solutions to take care of both low actuation voltage and temperature insensitivity, further research is still on the way.

Residual stress. Residual stress is introduced during manufacturing process. Generally, when we talk about residual stress, it refers to the intrinsic stress and thermal stress. Intrinsic stress is caused by the thin film deposition process. To date, there are no systematic theories to explain the cause of intrinsic stress. Generally, lattice mismatch, impurities introducing, lattice reconfiguration, and phase change will together contribute to the intrinsic stress. As far as we know, intrinsic stress is deposition technique dependent. It varies from different deposition processing parameters, and generally inevitable, and must be minimized by succeeding treatment, like rapid thermal annealing, etc.

In fixed-fixed beam structure, stresses inside the beam may cause buckling of the structure. Strain counteraction is an effective way to reduce the residual stress. By depositing a thin metallic film on the top of the membrane structure, and manipulating the process parameters, one can attain the opposite stress state within the metallic film in order to counterbalance the deformation that arises from thermal stress. Another way to decrease the residual stress is increasing the thickness of the membrane. However, a thicker membrane will definitely increase the corresponding pull-in voltage. Therefore, a

suitable membrane thickness with a beneficial actuation voltage should be carefully considered.

Furthermore, when the environmental temperature rises, the compressive stress inside the membrane will increase as well, which may reduce the restoring force of the membrane as a result. On the contrary, when the environmental temperature decreases, the tensile stress will increase correspondingly. It will lead to an increasing of the restoring force. However, when operational temperature varies, the switch geometry and residual stress vary accordingly, which makes the problem even more complicated.

In Chapter 4, we will discuss the cause of thermal stress in details with the knowledge of thermoelasticity, and then correlate it to the finite element analysis, in order to find out the beneficial stress within a suitable range of temperature.

4 Thermoelasticity Analysis

In RF MEMS switch, the membrane and the bottom electrode together construct a capacitor. Imagine that the metallic membrane with uniformly distributed temperature that has not been fixed to the anchors, when we decrease the temperature, the membrane will contract. On the contrary, when we elevate the temperature, the membrane will certainly extend. This is so-called the free expansion, and at this point, there is definitely no stress or strain generated in the membrane. However, when we fix two ends of the membrane to the anchors, and gradually decrease the temperature of the membrane, due to the existing constraints at both ends, the contraction of the membrane will be restrained. Therefore, the tensile stress will appear in the membrane. Similarly, when we elevate the temperature of the membrane, the expansion of the membrane will be hindered, and it will cause the compressive stress inside the membrane. As both of these two stresses are temperature dependent, they can be called as thermal stress.

Besides the aforementioned situations, there are some other methods that result in the thermal stress in the structures. As shown previously in Chapter 3, a mismatch between the thermal expansion coefficients of two materials will lead to thermal stress as well. When the temperature changes, the thermal strain in the membrane can be calculated by

$$\varepsilon_{th} = \int [\alpha_m(T) - \alpha_d(T)]dT \tag{4.1}$$

where $\alpha_m(T)$ and $\alpha_d(T)$ are the TCEs of membrane and dielectric, respectively. Thus, the thermal stress can be obtained by

$$\sigma_{th} = \left[\frac{E}{1-\nu}\right]\varepsilon_{th} \tag{4.2}$$

Here, E and ν are the elastic modulus and Poisson's ratio of the membrane, respectively. From Equation (4.1) and (4.2), we can see that, when the material properties of membrane and dielectric are known to us, the thermal stress are merely dominated by the temperature difference before and after the process. Commonly, the deposition process is done at very high temperature, e.g., at an elevated temperature of hundreds of degrees. Thus, when the device is cooling to the room temperature, there will be a large thermal stress generated in the membrane.

4.1 Thermoelastic Theory

Thermoelastic theory was created by J.M.C Duhamel in 1835, and developed by F. E. Neumann in 1841 [48]. For thermoelasticity, it contains two parts, the mechanical stress and strain that arising from the external force, and the thermal stress and strain that caused by variation of the temperature. To calculate the thermoelastic stress or strain, we can first use elasticity to solve for the stress and strain caused by the external force, and then employ thermoelastic principles to solve for the total thermal stress.

In a Cartesian coordinate system, we often use σ_{xx}, σ_{yy}, σ_{zz}, τ_{xy}, τ_{yz}, and τ_{zx} to describe the stress state of a single point of the analyzed object.

The thermoelastic equilibrium equation is

$$\frac{\partial \sigma_{xx}}{\partial x} + \frac{\partial \tau_{xy}}{\partial y} + \frac{\partial \tau_{xz}}{\partial z} + f_x = 0$$

$$\frac{\partial \sigma_{yy}}{\partial y} + \frac{\partial \tau_{yx}}{\partial x} + \frac{\partial \tau_{yz}}{\partial z} + f_y = 0 \quad (4.3)$$

$$\frac{\partial \sigma_{zz}}{\partial z} + \frac{\partial \tau_{zy}}{\partial y} + \frac{\partial \tau_{zx}}{\partial x} + f_z = 0$$

where u, v, and w are the displacements of the unit in x-, y-, and z-direction, respectively. f_x, f_y, and f_z are the components of body force in three orthogonal axes, respectively.

The variation of temperature will result in expansion of the object. If the thermal field varies with time, then the deformation of the object is a function of time as well. Therefore, an acceleration term will appear on the right-hand side of the equation. Thus, the Equation (4.3) becomes

$$\frac{\partial \sigma_{xx}}{\partial x} + \frac{\partial \tau_{xy}}{\partial y} + \frac{\partial \tau_{xz}}{\partial z} + f_x = \rho \frac{\partial^2 u}{\partial t^2}$$

$$\frac{\partial \sigma_{yy}}{\partial y} + \frac{\partial \tau_{yx}}{\partial x} + \frac{\partial \tau_{yz}}{\partial z} + f_y = \rho \frac{\partial^2 v}{\partial t^2} \quad (4.4)$$

$$\frac{\partial \sigma_{zz}}{\partial z} + \frac{\partial \tau_{zy}}{\partial y} + \frac{\partial \tau_{zx}}{\partial x} + f_z = \rho \frac{\partial^2 w}{\partial t^2}$$

The terms on the right-hand side are the inertia forces arising from the thermal deformation, where ρ is the material density of the object.

Due to the expansion nature of the material subjected to a temperature change, deformation of the material will occur, and the positions of the points in the material will be changed. Generally speaking, this deformation is barely visible, and the displacements

of the points are really quite small. Thus, we can obtain the strains by the geometric relationship between the points.

$$\varepsilon_{xx} = \frac{\partial u}{\partial x}$$

$$\varepsilon_{yy} = \frac{\partial v}{\partial y}$$

$$\varepsilon_{zz} = \frac{\partial w}{\partial z} \tag{4.5}$$

$$\gamma_{xy} = \frac{\partial u}{\partial y} + \frac{\partial v}{\partial x}$$

$$\gamma_{yz} = \frac{\partial v}{\partial z} + \frac{\partial w}{\partial y}$$

$$\gamma_{zx} = \frac{\partial w}{\partial x} + \frac{\partial u}{\partial z}$$

Considering the temperature involved in the calculation, for the isotropic material, the relationship between stress and strain is given by the generalized Hooke's Law (here, we use strains to express the stresses) [49, 50, 51]:

$$\sigma_{xx} = 2G[\varepsilon_{xx} + \frac{\nu}{1-2\nu}\epsilon - \frac{1+\nu}{1-2\nu}\alpha T]$$

$$\sigma_{yy} = 2G[\varepsilon_{yy} + \frac{\nu}{1-2\nu}\epsilon - \frac{1+\nu}{1-2\nu}\alpha T]$$

$$\sigma_{zz} = 2G[\varepsilon_{zz} + \frac{\nu}{1-2\nu}\epsilon - \frac{1+\nu}{1-2\nu}\alpha T]$$

$$\tau_{xy} = G\gamma_{xy} \tag{4.6}$$

$$\tau_{yz} = G\gamma_{yz}$$

$$\tau_{zx} = G\gamma_{zx}$$

where ν is Poisson's ratio, α is the linear thermal expansion coefficient, T is the temperature, E is the elastic modulus, G is the shear elastic modulus, $\epsilon = \varepsilon_{xx} + \varepsilon_{yy} + \varepsilon_{zz}$, called volume strain, and $G = E/2(1+\nu)$.

Including heat conduction equation (Fourier`s Law),

$$Q = -k\nabla T = -k\left(\frac{\partial T}{\partial x} + \frac{\partial T}{\partial y} + \frac{\partial T}{\partial z}\right) \tag{4.7}$$

where Q is the heat, k is the heat conductivity.

All together we have 16 equations for 16 unknown variables. Once we know the temperature distribution, we can obtain the strains by Equation (4-5), stresses can be easily solved by using Equation (4.2) [50, 51, 52].

4.2 Finite Element Method

Theoretically speaking, we can solve all the thermoelastic problems by employing equations listed above. However, in our practical work, the problems are much more complicated than we expected, and obtaining an analytical solution by hand sometimes seems impossible to us. Fortunately, the development of Finite Element method (FEM) provides us a better way to deal with these difficulties. By discretizing the analyzed area into finite elements, we can solve the problem point by point, and couple these solutions into the next analyzed area or elements. Therefore, we can obtain a whole solution

eventually. With the development of the computer science, FEM presents us a much wider application in our actual life.

Generally, finite element analysis (FEA) is proceeded in the following steps [53]:

(1) The discretization of the continuous object. This is the basic procedure in FEM. We must separate the continuous object into finite elements for the following calculation. The number of the elements and the element type we used to approach them will have great effects on the accuracy of the results. Commonly, line element is used in the discretion of 1-D structures. 2-D structures can be modeled by triangular or square element. And the element type in 3-D modeling can be tetrahedral or hexahedral.
(2) Selecting the model. In general, the hypothetical displacement function is a polynomial that only approaches the actual displacement. In practical application, there is no such function that perfectly matches the real displacement function. All we can do is to select the order of the polynomial so that in an acceptable calculating time, it can simultaneously satisfy the required accuracy, while meet the capability of the computer.
(3) Employing a variational method to deduce the stiffness matrix. The stiffness matrix consists of element material and the coefficients of the equilibrium equations based on the principle of minimum potential energy and some other principles. It is not only used to correlate the displacement of the body with the applied force/load, but also combines stress and strain together.
(4) Assemble the algebraic equations of the discrete objects. After the first three steps, we initially obtain the basic solution (stiffness matrix) of each nodes or elements.

Based on these results, FEM assembles the stiffness matrix of each element into the stiffness matrix of the whole continuous object, and assembles the node vectors of each element as the total load vector. And after obtaining the governing equations, we should also consider the initial conditions and boundary conditions, so that we can make the equations closed.

(5) Solve for these governing equations. After solving these governing equations, we can obtain the displacement vectors for the following calculation of the stress and strain.

(6) Deduce the corresponding stresses and strains based on the analytical results we obtained by the equations.

In practical work, these steps are only some of the basic procedures in the FEA by the computer. In order to complete the practical analysis, more preprocessing and postprocessing needs to be done before and after these procedures.

4.3 ANSYS Simulation

In our study, we employ ANSYS to simulate the thermal stress of the membrane. The applied formulas are showing below [7, 53].

Assuming that the material is linear elastic, and in order to simplify the tedious subscripts for each component, we can write the general matrix equation between stress and strain as

$$\begin{bmatrix} T_1 \\ T_2 \\ T_3 \\ T_4 \\ T_5 \\ T_6 \end{bmatrix} = \begin{bmatrix} C_{11} & C_{12} & C_{13} & C_{14} & C_{15} & C_{16} \\ C_{21} & C_{22} & C_{23} & C_{24} & C_{25} & C_{26} \\ C_{31} & C_{43} & C_{33} & C_{34} & C_{35} & C_{36} \\ C_{41} & C_{42} & C_{43} & C_{44} & C_{45} & C_{46} \\ C_{51} & C_{52} & C_{53} & C_{54} & C_{55} & C_{56} \\ C_{61} & C_{62} & C_{63} & C_{64} & C_{65} & C_{66} \end{bmatrix} \begin{bmatrix} s_1 \\ s_2 \\ s_3 \\ s_4 \\ s_5 \\ s_6 \end{bmatrix} \quad (4.8a)$$

In short-hand form, the expression is

$$\{T\} = [C]\{s_{el}\} \quad (4.8b)$$

Where the $\{T\}$=$[T_1, T_2, T_3, T_4, T_5, T_6]^{\mathrm{T}}$=$[\sigma_{xx}, \sigma_{yy}, \sigma_{zz}, \gamma_{xy}, \gamma_{yz}, \gamma_{zx}]^{\mathrm{T}}$, $\{s\}$=, the coefficient matrix [*C*] is called the stiffness matrix, as indicated in Section 4.2.

$\{s_{el}\} = \{s\} - \{s_{th}\}$, is the elastic strain matrix,

$\{s\} = [s_1, s_2, s_3, s_4, s_5, s_6]^T = [\varepsilon_{xx}, \varepsilon_{yy}, \varepsilon_{zz}, \tau_{xy}, \tau_{yz}, \tau_{zx}]^T$ is the total strain matrix, and

$\{s_{th}\}$ is the thermal strain matrix.

Equation (4.8b) can also be written with compliance matrix *S*, so that we can use the stress tensor to express the strain. In short-hand form, it is

$$\{s_{el}\} = [S]\{T\} \quad (4.9)$$

The compliance matrix [*S*] is the inverse of stiffness matrix [*C*] [7].

According to Equation (4.1), we can see that, for a 2-D model, $\{s_{th}\} = \Delta T[\alpha_x \quad \alpha_y]^T = (T - T_{ref})[\alpha_x \quad \alpha_y]^T$, where T_{ref} is the temperature when strain is zero, and *T* is the temperature that will be evaluated in FEA.

For a 3-D model, $\{s_{th}\} = \Delta T[\alpha_x \quad \alpha_y \quad \alpha_z \quad 0 \quad 0 \quad 0]^T$, and $\Delta T = T - T_{ref}$ as we indicated in 2-D model. $\alpha_i (i = x, y, z)$ denote the linear thermal expansion coefficient in x-, y- z- directions, respectively.

5 Finite Element Modeling of Thermal Stresses in Membranes

With the operation of the RF MEMS switch, charges will be built up in the dielectric layer, which will generate an additional "pull-in" voltage to hold the membrane in the "down" position. With increasing operating time, the degree of the dielectric charging will become more serious, which in turn decreases the release voltage. If the membrane still were held in its "down" position when the applied voltage has been completed removed, it is called stiction, and represents a failure of the device. In this situation, two questions are worth considering. One is the shift of C-V curve, and another is the method to overcome this stiction effect.

As we discussed in the last chapter, within a certain range of temperature, the thermal stress can make a great contribution to the restoring force. Fig.5-1 shows the schematic analysis of thermal stress behavior when stiction occurs.

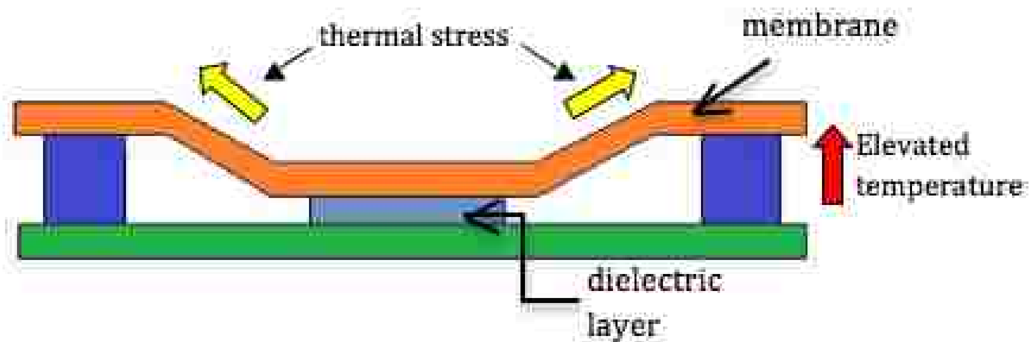

Fig.5-1 Schematic diagram of capacitive switch with elevated temperature

When stiction happens, the built-up charges in the dielectric layer will lead to a persistent voltage to restrain the membrane in its down state, even though the applied

voltage has been removed. When examining the C-V curve, it represents the shift of the curve, specifically the superposition of the release voltage curve and Y-axis, as shown in Fig.5-2.

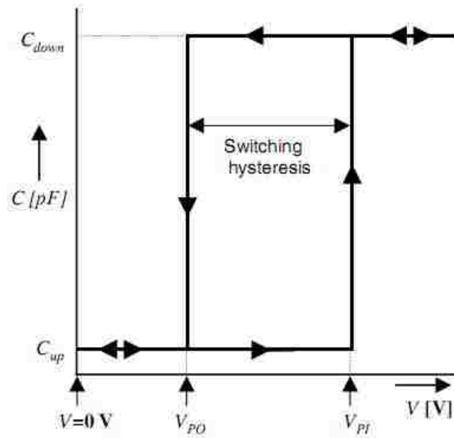

Fig.5-2 Shifting of C-V curve [54]

In this chapter, our effort mainly focuses on employing ANSYS to simulate the variation or trends of thermal stress inside the membrane, with gradually increasing temperature. Subsequently apply this Temperature-Thermal Stress curve to calculate the electrostatic force, in order to find the release voltage, or predicting the shift of the C-V curve.

5.1 Finite Element Modeling of Membrane Thermal Stress

There are various commercial software capable of simulating the thermal analysis, structural analysis, electromagnetic analysis, and dynamic analysis of the designed components. Generally, COMSOL, ANSYS, ABQUS, and AUTODESK ALGOR are the most popular simulation codes among numerous products. Furthermore, ANSYS

has its unique benefits over other simulation products. It can attain multi-fields coupling, co-operative simulation, two-way interaction, effective parallel computing, etc. In this section, we employ ANSYS to help us simulate the membrane thermal stress with a gradually elevated temperature, in which way providing us an simple way to approximately predict the release voltage and the charge density of the switch, which are characteristic for the steady state behavior of a RF-MEMS capacitive switch.

Finite element simulations were performed for RF MEMS switch structure in 2D and 3D, respectively. As the width of the membrane is much larger than its thickness, i.e., w>>t, we can use 2D models to simulate the thermal stress in the membrane. Moreover, in order to verify the accuracy of the simulation results, we also apply 3D model here, and compare the results we obtained between 2D and 3D models.

The critical parameters used in the simulation, including the gap spacing, thickness and length of membrane, Young`s modulus, Poisson ratio, etc., are listed in Table.5-1.

Table.5-1 Critical parameters of RF MEMS membrane (Au)

Poisson`s Ratio	ν	0.42
Thermal Expansion Coefficient	α	14.2 μm/mK
Density	ρ	19300 kg/m^3
Specific Heat	C	130.5 J/kg℃
Thermal Conductivity	K	315W/mK
Dimension of Membrane	X/Y/Z	320 μm/0.3 μm/100 μm

Dimension of Dielectric	X/Y/Z	90 μm/0.28 μm/180 μm
Gap	G	4μm

It should be noted that Young`s modulus varies with temperature. Table.5-2 lists the different Young`s moduli at different temperature [55, 56]. For more details on the determination of Young`s modulus, see the Appendix.

Table.5-2 Young`s modulus of Au in different temperature

Temperature	Young`s Modulus	Temperature	Young`s Modulus
-50	78.974GPa	50℃	76.134GPa
-40	78.690GPa	80℃	75.282GPa
-30	78.406GPa	90℃	74.998GPa
-20	78.122GPa	100℃	74.714GPa
-10	77.838GPa	120℃	74.146GPa
0	77.554GPa	150℃	73.294GPa
10	77.270GPa	180℃	72.442GPa
20℃	76.986GPa	200℃	71.874GPa
30℃	76.702GPa		

2-D Modeling of Membrane Thermal Stress

The 2-D RF MEMS membrane modeling was performed using ANSYS. In order to incorporate the analysis of thermal stress in 2-D problem, PLANE77 was used in this simulation. PLANE77 is a 2-D element with 8 nodes, and each node only has one

degree of freedom, i.e., temperature. All the nodes have uniform temperature function, which makes it more suitable for modeling the structure with curve edges, and for static state or transient state problems as well [57].

As the modeling of membrane thermal stress involves two fields, thermal issues and structural analysis, ANSYS offers us two powerful methods to solve this kind of problems, which are direct-simulation and indirect-simulation [58].

Direct-simulation: Applying the coupled element with temperature and displacement DOFs, and obtaining the thermal analysis results and structural stress analysis results simultaneously.

Indirect-simulation: First conducting the thermal analysis, and subsequently applying the thermal analysis results as the loads in the analysis of structure stress.

As all the features of thermal analysis and structural analysis can be involved in the indirect-simulation method, it is recommended for most coupled-fields problems. If the analyzed thermal problem referring to transient state, the only thing we need to know is the time point when the structure has its greatest temperature gradient, and applying this nodal temperature as the loads onto the structural stress analysis.

In this case, we choose indirect-simulation method. As aforementioned, we select PLANE77 for the element type, and first setting 20℃ to be the membrane`s initial temperature. After obtain the temperature solution of the whole structure, we switch to the structural analysis, and apply the thermal solution as the load to the upcoming simulation. For this step, the element type was changed to PLANE183. PLANE183 is a higher order 2-D element with 8 nodes. It has quadratic displacement behavior and is capable of modeling irregular meshes, plasticity, creep, stress stiffening, large

strain, etc. Here we set all DOFs of the two ends of the membrane to be 0, while the displacement in Y direction of middle part of the membrane was set to be -4μm, to simulate the time when the membrane was tightly attached to the bottom electrode. Now we can solve for the thermal stress inside the membrane in such static state situation.

In order to get close to the development of thermal stress under different temperature, we can easily calculate them by only revising the temperature value in the APDL codes we wrote in the previous simulation, and increasing this value by 10℃ per simulation. By comparing the thermal stress distribution under various temperatures, we may obtain a general idea of temperature dependent thermal stress variation. Specifically, we can select one node and analyze its stress development with temperature. In our case, we choose node 2395 to study. The following figures, Fig.5-3, Fig.5-4, Fig.5-5, Fig.5-6, represent the thermal stress of the membrane with the applied temperature of 27℃, 50℃, 100℃, and 150℃, respectively. As reported in Ref.[43], since the bottom electrode only served only as a applied load (pull-in force), we didn't mesh the bottom electrode, and the membranes appeared in these figures are considered to be contacted the bottom electrode.

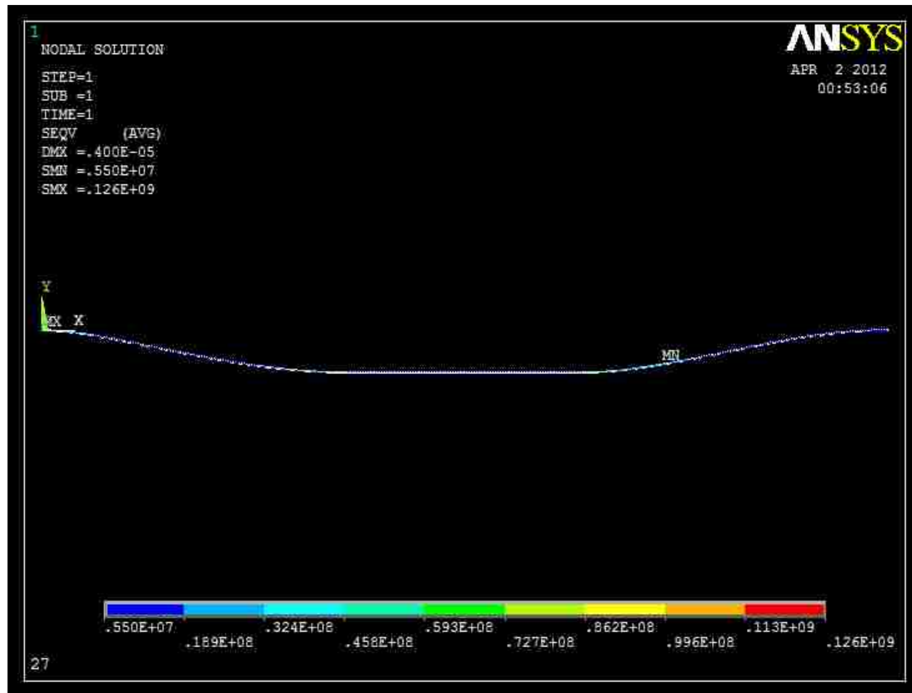

Fig.5-3 Thermal stress of the membrane with an applied temperature of 27℃

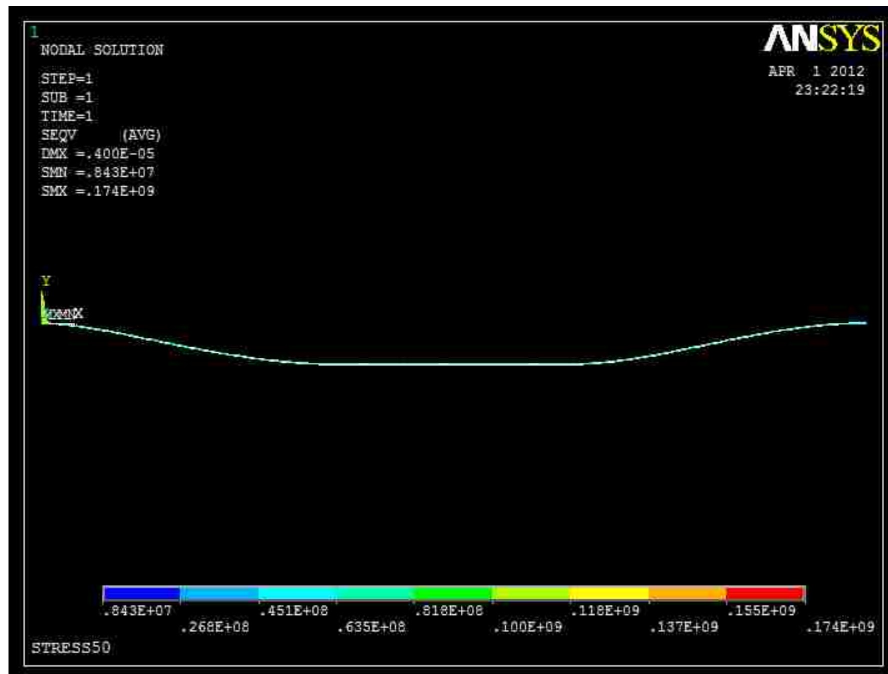

Fig.5-4 Thermal stress of the membrane with an applied temperature of 50℃

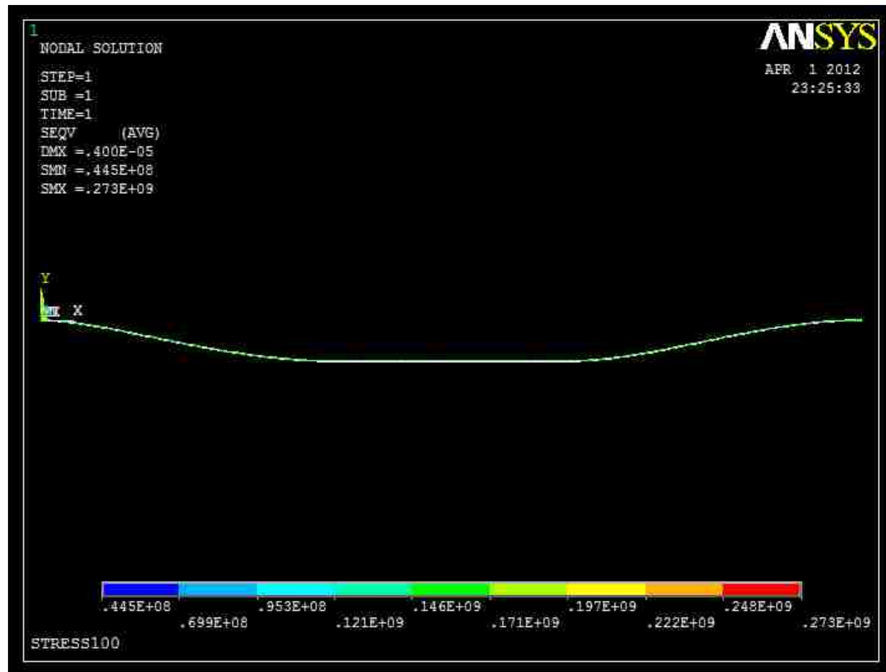

Fig.5-5 Thermal stress of the membrane with an applied temperature of 100°C

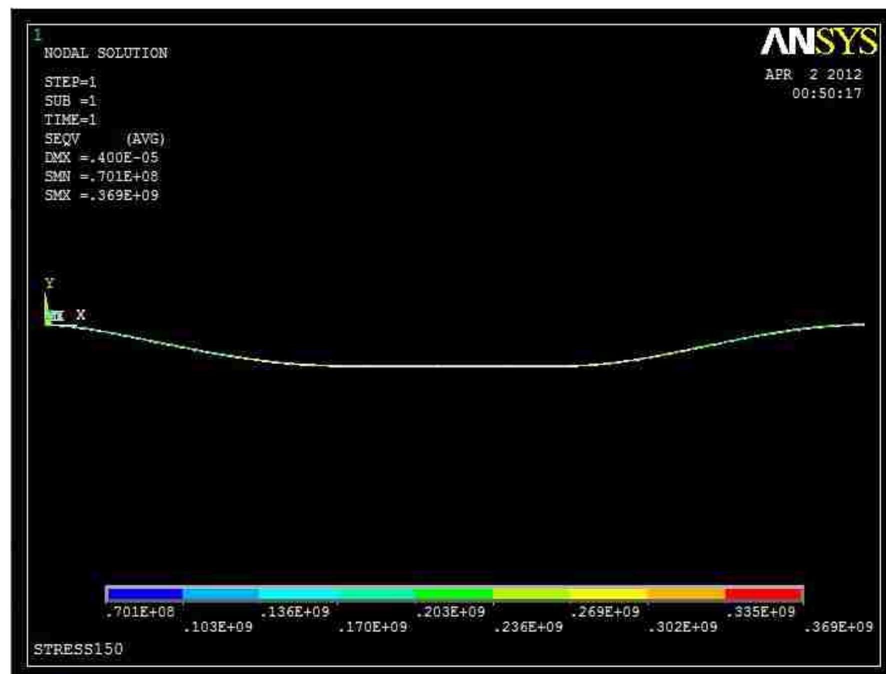

Fig.5-6 Thermal stress of the membrane with an applied temperature of 150°C

Fig.5-7 shows the variation of compressive stress of node 2395 with increasing temperature.

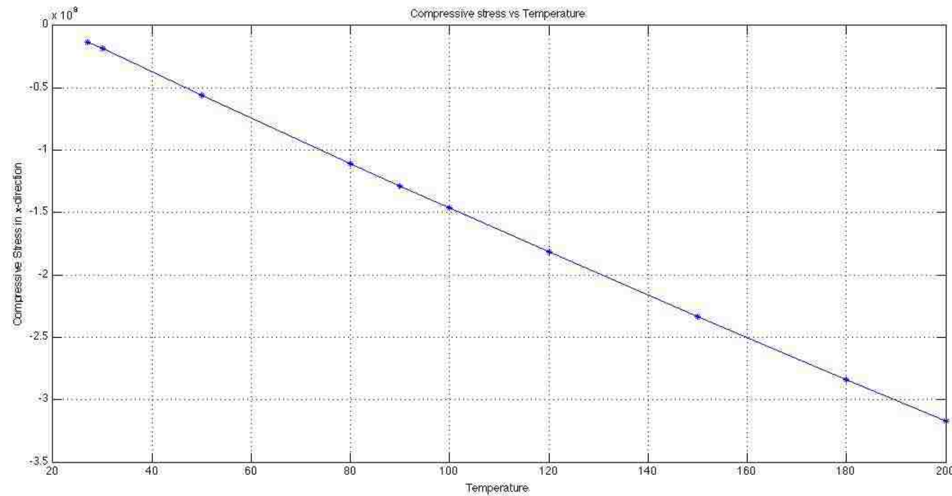

Fig.5-7 Compressive Stress of node 2395 vs Temperature

Through Fig.5-3 to Fig.5-6, we can see that, the parts near two anchors exhibit higher stress state than the central part, which may be due to their larger deformation when compared with the central part of the membrane. And from Fig.5-7, we can even more directly find out the relationship between temperature and thermal stress. We can see that, with the temperature increasing gradually, the compressive stress gets lower and lower correspondingly.

It can be seen that, when we increase the temperature of the structure, the accompanied absolute value of the compressive stress increases as well, which in turn decreases the restoring force of the membrane to counterbalance the sticking force generated by dielectric charging, and will hinder the release of the membrane to its original state (“UP” state).

However, when we decrease the temperature, the tensile stress will develop in the

membrane, which can increase the restoring force and overcome the stiction. Fig.5-8 shows the development of the tensile stress vs decreasing temperature.

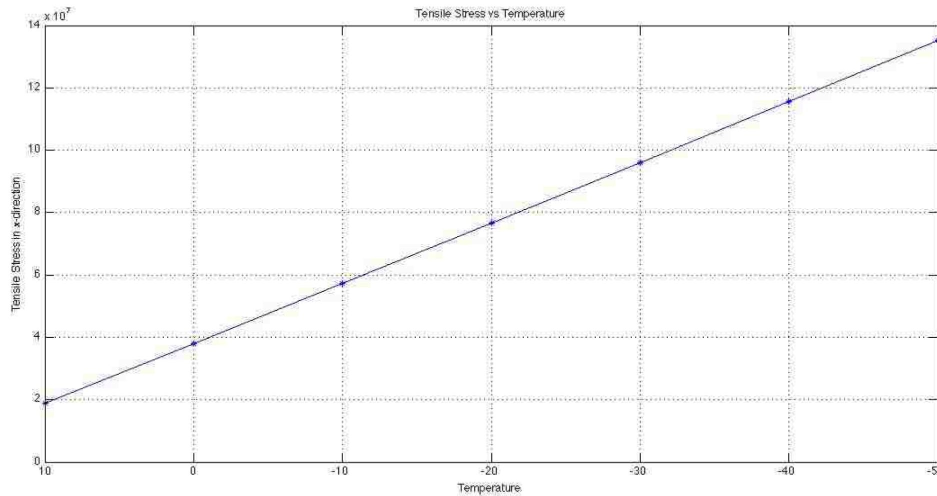

Fig.5-8 Tensile stress of node 2395 vs Temperature

Ultimately, we can apply these models to obtain the relationship between the temperature and the dielectric charging caused voltage, so that we can find out the approximate release voltage of the RF MEMS device under different temperature. Before we looking for the release voltage of the switch, we will conduct a 3-D modeling of thermal stress inside the membrane to verify the relationship we obtained by 2-D modeling. Afterwards, the last section of this chapter will be talked about the analytical model of release voltage and C-V curve shift of RF MEMS switches.

3-D Modeling of Membrane Thermal Stress

In the last section, we mainly talked about the 2-D modeling of RF MEMS switch, and found out the relationship between the temperature and the thermal stress. In this section, we use 3-D modeling of the RF MEMS switch to verify the accuracy of the 2-D model. The dimension and the material properties are the same with 2-D model,

and basically the modeling process of 3-D simulation is similar with 2-D model as well. In 3-D modeling, we choose SOLID70 as the element type. SOLID70 is a hexahedral element with 8 nodes, and each node has the DOF of temperature.

We also choose indirect analysis here to calculate the thermal stress of the structure. As usual, we still start with the analysis of the thermal field. After we obtain the temperature of the nodes, we apply these results as the loads to the structural analysis. Here, the element type switches to SOLID186, which is a higher order 3-D 20-node solid element that exhibits quadratic displacement behavior.

It should be noted here that, as the thickness of the membrane is only $0.3\mu m$, which is much smaller comparing with its length and width, the meshing process is more complicated than 2-D modeling. Thus, we use sweeping to help us constructing the mesh with more regular shape and size.

The following figures exhibit the displacement and the Von Mises stress of the membrane under different temperature, respectively.

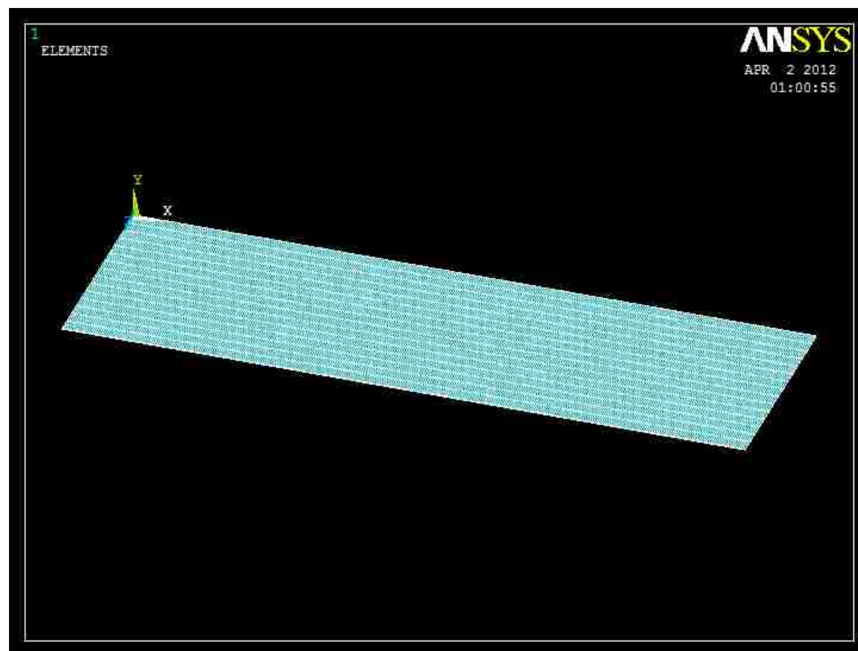

(a)

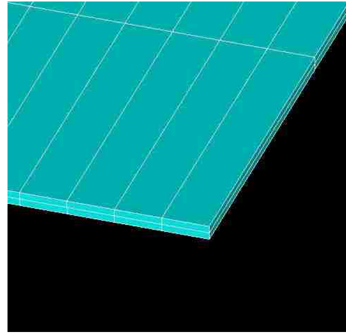

(b)

Fig.5-9 (a) Finite element meshing of the membrane; (b) Zoom in view of the corner of the meshed membrane

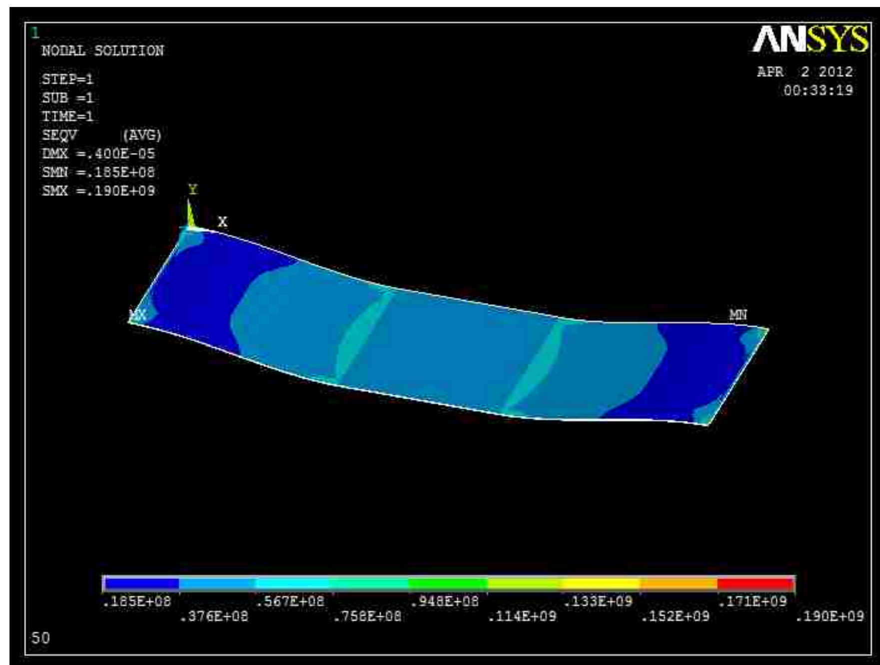

Fig.5-10 The Von Mises stress of the membrane with the applied temperature of 50℃

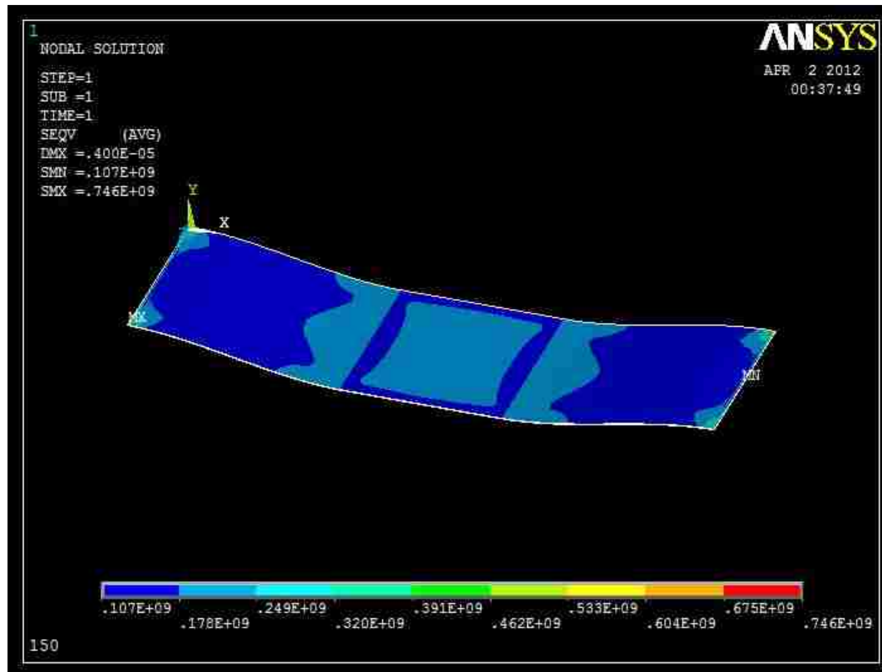

Fig.5-11 The Von Mises stress of the membrane with the applied temperature of 150℃

By investigating Fig.5-4, Fig.5-6, Fig.5-10, and Fig.5-11, we can see that, the Von Mises stresses we obtained by 3-D modeling are a little bit smaller than 2-D modeling. However, the relative error $\delta = \frac{s1-s2}{s1} = \frac{(0.451-0.376)\times 10^8}{0.451\times 10^8} \times 100\% = 16.6\%$, is relatively small enough, which verifying that the 2-D model shows a good match to 3-D FEA simulation (Here, the data are selected near node 2395 in 3-D modeling and 2-D modeling under 50℃, respectively).

Now, we can use the results obtained by 2-D modeling to solve for the electrostatic force generated by dielectric charging, so that we could find out the release voltage we need to set the membrane freely to its original position under different temperature.

5.2 Analytical Model of release voltage of RF MEMS Switches

When we apply a voltage between the membrane and the bottom electrode, the membrane will deform towards the bottom electrode due to the electrostatic force, as shown in Fig.5-12 [10].

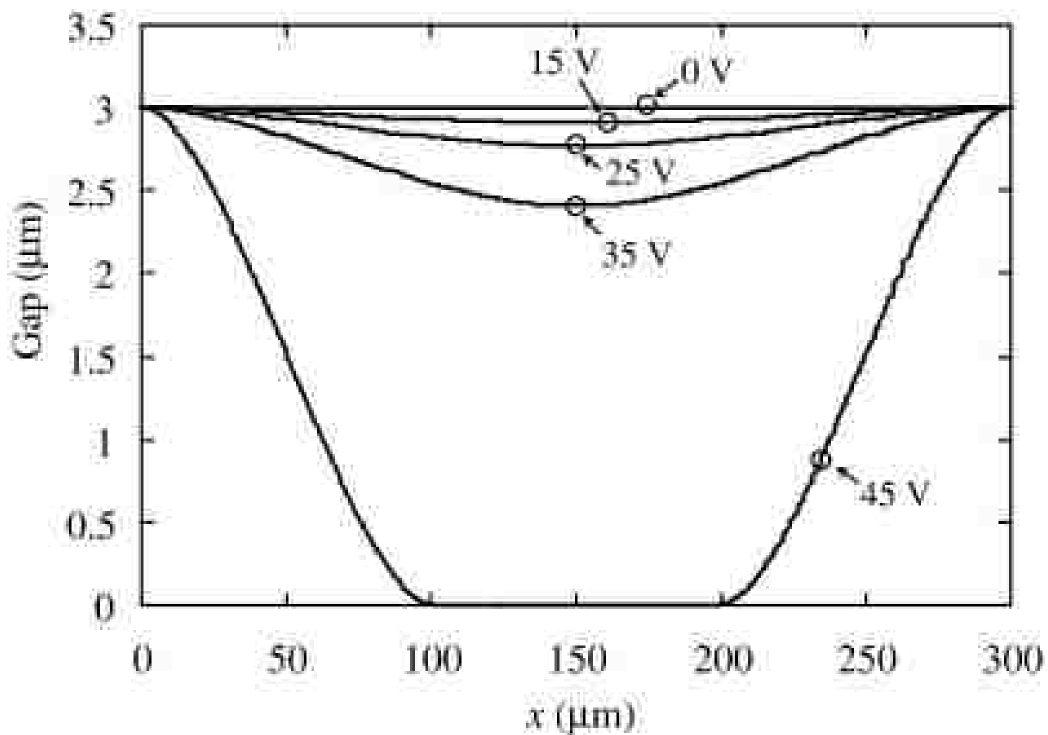

Fig.5-12 Shape of a fixed–fixed beam for different actuation voltages

Once the voltage reaches a certain value, the membrane suddenly deflected to the bottom and sticks to it. When we diminish the applied voltage to a certain value, the membrane will spring back to its initial position. The C-V curve is shown in Fig.5-13.

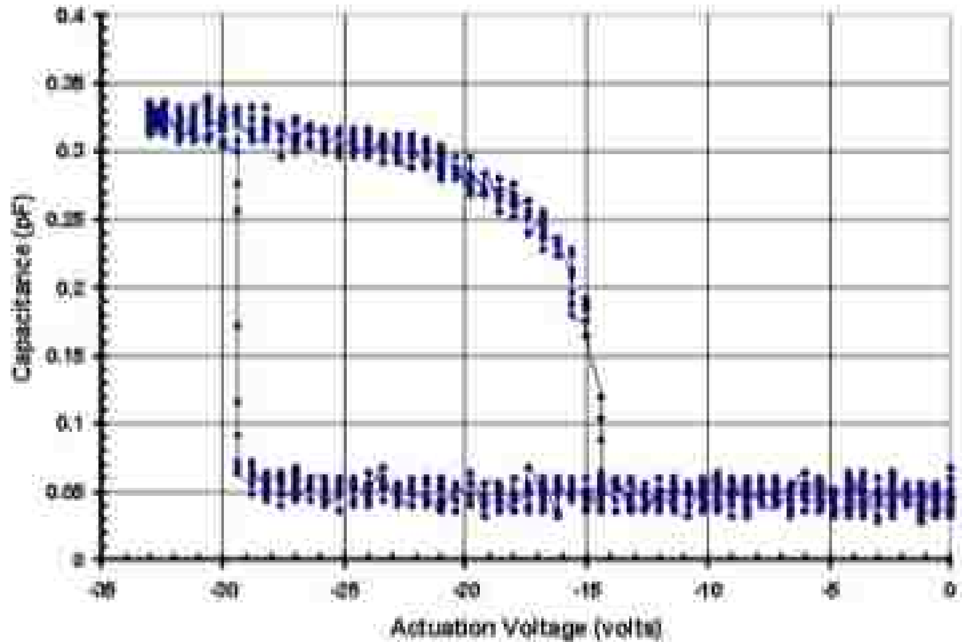

Fig.5-13 C-V curve of RF MEMS switch [59]

However, with the dielectric charging progressing, the release voltage gradually drops. Even when we remove the actuated voltage, the membrane may still be stuck to the dielectric layer, i.e., stiction has occured. At this point, the voltage generated by the charges is equal to the release voltage, and the membrane is in an equilibrium state, in other words, the electrostatic force, F_e, equals the supporting force offered by the dielectric layer, F_N, and the restoring force of the membrane, F_r, as shown in Equation 5.1.

$$F_e = F_N + F_r \tag{5.1}$$

When we decrease the temperature of the membrane, the tensile stress of the membrane will increase, which in turn increases the restoring force, as shown in

Fig.5-9. Once the membrane is about to spring back to its original position, F_N will disappear, and Equation 5.1 is simplified to Equation 5.2.

$$F_e = F_r = F_{release} \tag{5.2}$$

By looking up to the temperature-stress curve, we can find out the release force, $F_{release}$ under the certain temperature.

While the switch is in its "down" state, the equivalent capacitance model is shown in Fig.5-14. Here we assume that the charges uniformly distribute in the middle of the dielectric layer, so the space of the capacitance is half of the layer.

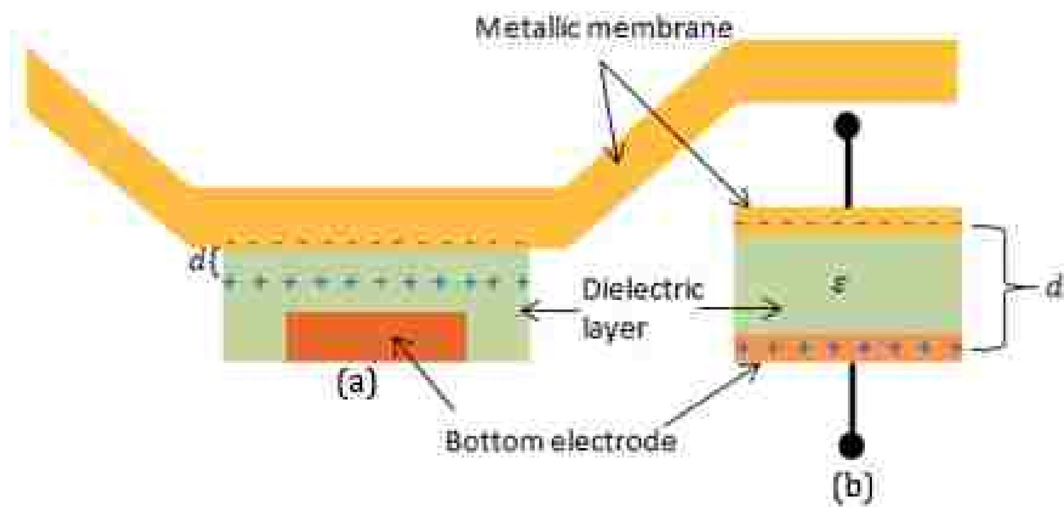

Fig.5-14 Equivalent capacitance model of the switch. (a) shows the charge distribution in the membrane and dielectric layer; (b) equivalent capacitance of the "DOWN" state

The capacitance between two parallel plates is defined as

$$C = \frac{Q}{V} \tag{5.3}$$

where Q is the amount of stored charges and V is the applied voltage. The electric energy U in the capacitor is defined as

$$U = \frac{1}{2}CV^2 = \frac{1}{2}\frac{Q^2}{C} \tag{5.4}$$

Based on Gauss's law, the value of the electric field E is

$$E = \frac{Q}{\varepsilon A} \tag{5.5}$$

As the voltage is the electric field times the spacing between two parallel plates, thus, the capacitance can be calculated by

$$C \equiv \frac{Q}{V} = \frac{Q}{E \cdot d} = \frac{Q}{\frac{Q}{\varepsilon A}d} = \frac{\varepsilon A}{d} \tag{5.6}$$

Therefore, the expression for the magnitude of the force F is [7]

$$F = \left|\frac{\partial U}{\partial d}\right| = \frac{1}{2}\left|\frac{\partial C}{\partial d}\right|V^2 = \frac{1}{2}\frac{\varepsilon A}{d^2}V^2 = \frac{1}{2}\frac{CV^2}{d} \tag{5.7}$$

Here, d represents the distance between the two parallel plates.

Combining Equation (5.2), Equation (5.6) and Equation (5.7), we can solve for the voltage generated by dielectric charging effect.

$$V_{release} = \sqrt{\frac{2dF_{release}}{C}} = \sqrt{\frac{2dF_{release}}{d/\varepsilon A}} = \sqrt{\frac{2F_{release}}{\varepsilon A}} \tag{5.8}$$

As defined previously, $F_{release}$ is the critical force that occurs when the membrane is about to spring back, or the electrostatic force equals the restoring force. Thus, we can relate the release voltage to the temperature, as described in Equation (5.9).

$$V_{release} \propto \sqrt{F_r(t)} \tag{5.9}$$

Here, t represents the temperature of the membrane, and $F_r(t)$ denotes a temperature dependent restoring force of the membrane.

Furthermore, we could utilize the thermal stress to calculate the charge density at any time before the occurring of the stiction.

When the applied voltage is large enough, the membrane will remain in its “down” state, which means the electrostatic force is bigger than the restoring force, i.e., $F_{a-v} + \Delta F_{charge} > F_r'$, where F_{a-v} denotes the electrostatic force contributed by the applied voltage, ΔF_{charge} denotes the electrostatic force contributed by the charges, and F_r' represents the initial restoring force of the membrane, i.e., at the time we haven`t apply the higher temperature on the membrane. Here, the applied voltage and the dielectric charging together contribute to the electrostatic force.

With rising up the temperature, the thermal stress in the membrane increases as well, which adds an additional force, $\Delta F_{thermal}$, to the membrane. With the operation of the switch, the degree of dielectric charging increases, and ΔF_{charge} becomes large as well. When the temperature increases to a certain value, the

membrane is about to spring back, and under such circumstance, we can obtain the following equation.

$$F_{a-v} + \Delta F_{charge} = F_r' + \Delta F_{thermal} = F_r \quad (5.10a)$$

or,

$$\Delta F_{charge} = F_r - F_{a-v} = \Delta F \quad (5.10b)$$

Also,

$$\Delta F_{charge} = Q \cdot E = Q \cdot (E_{a-v} + E_{charge}) = Q \cdot \left(E_{a-v} + \frac{Q}{\varepsilon A}\right) \quad (5.11)$$

$$= \delta \cdot A \cdot \left(\frac{V_{a-v}}{d} + \frac{\delta A}{\varepsilon A}\right) = \frac{\delta^2 A}{\varepsilon} + \frac{\delta A V_{a-v}}{d}$$

where δ is the surface charge density and A is the contacting area. Therefore, we have

$$\Delta F = \Delta F_{charge} = \frac{\delta^2 A}{\varepsilon} + \frac{\delta A V_{a-v}}{d} \quad (5.12a)$$

or,

$$\delta = \frac{\varepsilon}{2}\left(\sqrt{\left({V_{a-v}}/{d}\right)^2 + {4\Delta F}/{A\varepsilon}} - \frac{V_{a-v}}{d}\right) \quad (5.12b)$$

Here, F_{a-v} can be easily calculated by Equation (5.7), and $\Delta F_{thermal}$ can be directly found out by looking up to the temperature-stress curve. Therefore, we could estimate the dielectric charging degree by finding out the temperature

dependent variable, ΔF, in the temperature-stress curve.

Moreover, when the applied voltage decreases to zero, i.e., we have removed the applied voltage, F_{a-v} becomes zero, and stiction occurs. At this time, Equation (5.10) is the same with Equation (5.2), and we can also use Equation (5.12b) to calculate the charge density under this situation.

5.3 The Effects of Dielectric Layer Geometry on RF MEMS Switch Capacitance

Generally, there are two ways to counterbalance the stiction effect. One is increasing the restoring force of the membrane, another is diminishing the charging and moisture effect. The previous section presented a method to enhance the restoring force. Here, we will talk about another solution that can help us decreasing the stiction effect.

As discussed in Section 1.4, the charging effect, moisture of the working environment, and the molecular Van der Waals force are the major reasons that lead to the stiction failure. By carefully investigating of these three factors, we can find that, all these effects are related to the contacting area between the membrane and the dielectric layer.

The capillary force arises from the moisture environment. According to the principle of minimum total potential energy, the liquid always trends to stay in a state with minimum potential energy. As shown in Fig 5-15, the surface tension keeps the

dewdrop in the globular shape, in thus keeping the liquid under its minimum potential energy state.

Fig.5-15 Dewdrops on lotus leaf

In Section 1.2.2, we mentioned that, the surface tension becomes the overarching factor in MEMS area, which has the great effect on these miniature devices. In general, the membrane of the switch is about 0.2~0.4μm. Thus, in a moisture environment, the membrane will easily stick to the surface of the dielectric layer due to the existing liquid between them.

As covalent bonds, ion bonds, metallic bonds, and hydrogen bonds, Van der Waals force is also an intermolecular force that extensively existing in the nature. Van der Waals force consists of three force, Keesom force (orientation force)[60], Debye force (induction force) [61], and London dispersion force [62]. The interactional potential energies of these forces are all proportional to $1/r^6$, where r is the distance

between two molecules. Therefore, when the membrane and the dielectric layer has gotten close enough, the Van der Waals force will hamper the membrane from springing back.

Both these two forces directly depend on the contacting area. When the contacting area decreases, the amount of the liquid existing on the surface and the molecules of the dielectric that are closed to the membrane will be reduced, which in turn reducing the capillary force and Van der Waals forces simultaneously.

For the electrostatic force that arises from the dielectric charging, the situation will be more complicated.

As the electrostatic force between the metallic membrane (upper electrode) and the bottom electrode depends on the area of these electrodes, revising the geometry will not affect the total area of the electrode. This means the electrostatic force does not depend on the contacting area as directly as capillary force and Van der Waals force. However, by reducing the contacting area, we introduce some air to replace the dielectric, which will decrease the capacitance, and the electrostatic force as well.

Here, we calculate two different kinds of dielectric profile, and obtain the relationship between the contacting area ratio and the electrostatic force.

Corrugated Profile of Dielectric Layer

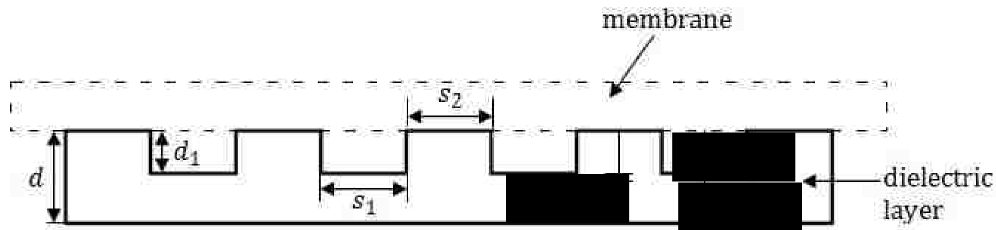

Fig.5-16 Corrugated profile of the dielectric layer

As we discussed in Section 5.2, the original switch without the corrugations in the dielectric layer has its capacitance as

$$C \equiv \frac{\varepsilon A}{d} \tag{5.6}$$

here, d is the thickness of the dielectric layer, A is the contacting area between membrane and the dielectric layer, and ε is the permittivity.

However, when we make some corrugation profile on the dielectric, we introduce some air inside, which replaces the previous dielectric and reduces the capacitance of the whole system.

For $C_{original}$, it is the same with the previous calculation, as

$$C_{original} = \frac{\varepsilon S_2}{d} = \frac{\varepsilon_0 \varepsilon_r S_2}{d} \tag{5.13}$$

here, ε_0 is the permittivity of the air, and ε_r is the relativity of the dielectric.

To simplify the analysis, we first assume that the depth of the corrugation d_1 is half of the whole thickness of the dielectric layer. Therefore, we can easily find out the capacitance C_1 and C_2.

$$C_1 = \frac{\varepsilon_0 S_1}{d/2} = \frac{2\varepsilon_0 S_1}{d} \tag{5.14}$$

$$C_2 = \frac{\varepsilon_0 \varepsilon_r S_1}{d/2} = \frac{2\varepsilon_0 \varepsilon_r S_1}{d} \tag{5.15}$$

As the equivalent capacitors C_1 and C_2 are in the series connection, the total capacitance is:

$$C_{corrugated} = \frac{C_1 C_2}{C_1 + C_2} = \frac{2\varepsilon_0 \varepsilon_r S_1}{d(1+\varepsilon_r)} \tag{5.16}$$

Assume that $\frac{\sum S_1}{A} = \alpha$, and $\frac{\sum S_2}{A} = \beta$. Apparently, we have $\alpha + \beta = 1$. And $C_{original}$ and $C_{corrugated}$ are in shunt connection. Thus, we can solve for the total electrostatic force on the switch based on Equation (5.7).

$$F_{electr} = \frac{1}{2}\frac{CV^2}{d} = \frac{1}{2}\frac{[\sum C_{original} + \sum C_{corrugated}]V^2}{d} \tag{5.17}$$

$$= \frac{1}{2}\frac{V^2}{d}\left[\frac{2\varepsilon_0\varepsilon_r\alpha A}{d(1+\varepsilon_r)} + \frac{\varepsilon_0\varepsilon_r\beta A}{d}\right]$$

$$= \frac{1}{2}\frac{\varepsilon_0\varepsilon_r A V^2}{d^2}\left[\frac{2\alpha}{(1+\varepsilon_r)} + 1 - \alpha\right]$$

$$= \frac{1}{2}\frac{\varepsilon_0\varepsilon_r A V^2}{d^2}\left[1 - \frac{\alpha(\varepsilon_r - 1)}{\varepsilon_r + 1}\right]$$

Therefore, we can compare the electrostatic forces between the original switch and the revised profile switch.

$$\eta = \frac{F_{electr}}{F_{orignial}} = \frac{\frac{1}{2}\frac{\varepsilon_0 \varepsilon_r A V^2}{d^2}\left[1 - \frac{\alpha(\varepsilon_r - 1)}{\varepsilon_r + 1}\right]}{\frac{1}{2}\varepsilon_0 \varepsilon_r A \left(\frac{V}{d}\right)^2} = 1 - \frac{\alpha(\varepsilon_r - 1)}{\varepsilon_r + 1} \tag{5.18}$$

For instance, when $\alpha = 0.5$, which means there are half area of the dielectric layer has been fabricated with corrugation, and at this time, the electrostatic force has dropped to 65% of the original force.

Semispherical Profile of the Dielectric Layer

From the above analysis, we can see that, when we reduce the contacting area, or said, ratio β, we can reduce the electrostatic force dramatically.

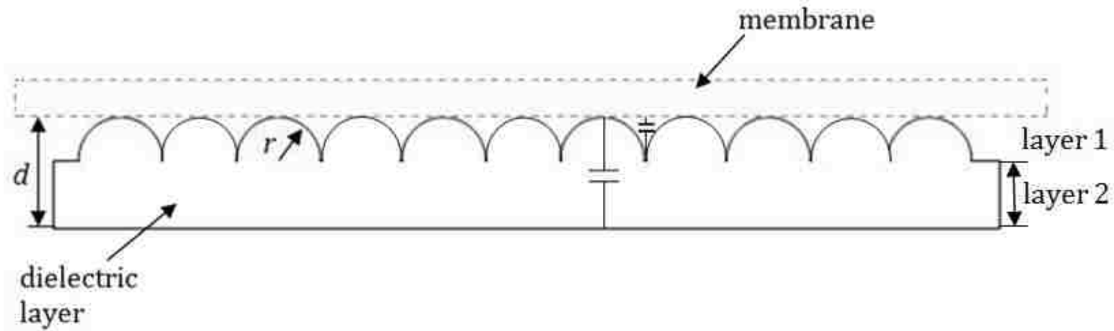

Fig.5-17 Semispherical profile of the dielectric layer

Here, we bring up a different design of the dielectric layer profile, with hemisphere array on it. For this structure, we change the area-contact into point-contact, which will further reducing the contacting area.

For this shape, the calculation of the capacitance will be more complicated than corrugated shape. A wise strategy is separating the array into discrete cubes and solve for their capacitances respectively, and them sum them up. Fig.5-18 shows the strategy that separating the cubic unit into two parts, cylinder part and four-corner part. In the four-corner districts, blue highlights the air in it. In the cylinder region, it contains two materials: inside the hemisphere it is the dielectric layer, outside the hemisphere it is also air. When we calculate the whole capacitance of this cubic unit, we should solve for each capacitances separately. First, inside the cylinder, the air part and the dielectric part are in series connection. And then for the whole unit, the cylinder and the four-corner are in the shunt connection.

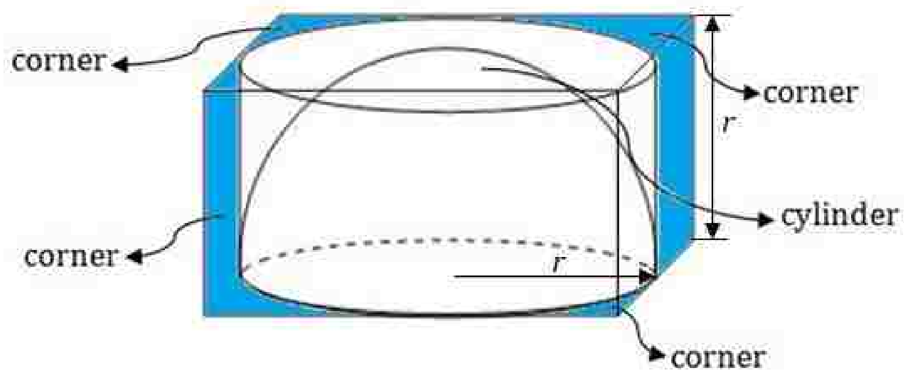

Fig.5-18 Separation of the unit

Fig.5-19 shows the schematic of discrete cubic unit of layer 1.

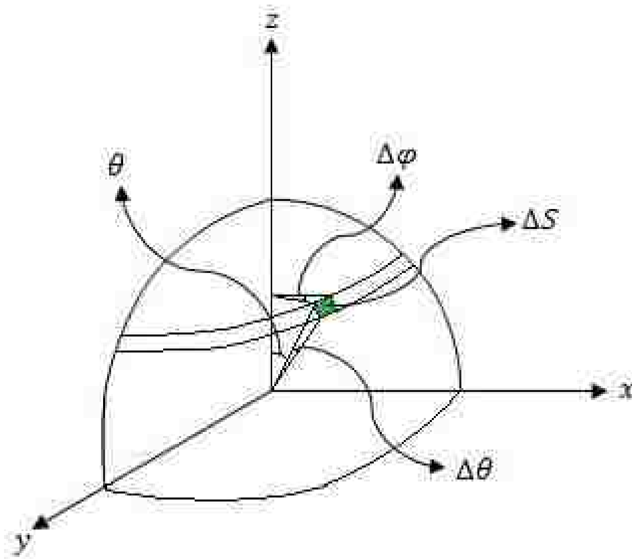

Fig.5-19 Schematic of the discrete cubic unit

In Fig.5-19, $\Delta S = (r sin\theta \Delta\varphi) \cdot (r\Delta\theta) = r^2 sin\theta \Delta\theta \Delta\varphi$, when $\Delta S \rightarrow 0$, we can rewrite ΔS as $dS = r^2 sin\theta d\theta d\varphi$. Therefore, the capacitance on this extremely small area will be the combination of $C_{air}(dS)$ and $C_{dielectric}(dS)$.

$$C_{air}(dS) = \frac{\varepsilon_0 dS}{r(1 - cos\theta)} \tag{5.19}$$

$$C_{dielectric}(dS) = \frac{\varepsilon_0 \varepsilon_r dS}{r cos\theta} \tag{5.20}$$

$$C(dS) = \frac{C_{air}(dS) C_{dielectric}(dS)}{C_{air}(dS) + C_{dielectric}(dS)} \tag{5.21}$$

$$= \frac{\varepsilon_0 \varepsilon_r dS}{r[cos\theta + \varepsilon_r(1 - cos\theta)]}$$

For the total capacitance of this cubic unit, we have two part: $C_{\text{semisphere}}$ and C_{corner}.

$$C_{\text{semisphere}} = \sum C(dS) = \int C(dS) \tag{5.22}$$

$$= \int_{\varphi=0}^{2\pi} \int_{\theta=0}^{\frac{\pi}{2}} \frac{r^2 \varepsilon_0 \varepsilon_r sin\theta d\theta d\varphi}{r[cos\theta + \varepsilon_r(1 - cos\theta)]}$$

$$= r\varepsilon_0\varepsilon_r \int_0^{2\pi} d\varphi \int_0^{\frac{\pi}{2}} \frac{sin\theta d\theta}{cos\theta + \varepsilon_r(1 - cos\theta)}$$

$$\xRightarrow{t=cos\theta} 2\pi r\varepsilon_0\varepsilon_r \int_0^1 \frac{dt}{\varepsilon_r + (1 - \varepsilon_r)t}$$

$$= \frac{2\pi r\varepsilon_0\varepsilon_r}{1 - \varepsilon_r} \ln[(1 - \varepsilon_r)t + \varepsilon_r]_0^1 = \frac{2\pi r\varepsilon_0\varepsilon_r \ln(\varepsilon_r)}{\varepsilon_r - 1}$$

$$C_{corner} = \frac{\varepsilon_0[(2r)^2 - \pi r^2]}{r} = \varepsilon_0(4 - \pi)r \tag{5.23}$$

$$C_{layer_1} = C_{\text{semisphere}} + C_{corner} \tag{5.24}$$

$$= \frac{2\pi r\varepsilon_0\varepsilon_r \ln(\varepsilon_r)}{\varepsilon_r - 1} + \varepsilon_0(4 - \pi)r$$

By carefully choosing the parameter *r*, we can have the dielectric layer occupied by $m \times n$ cubic units, where m and n are both integers.

For layer 2, the capacitance can be easily found out, as $C_{layer_2} = \frac{4\varepsilon_0\varepsilon_r r^2}{d-r}$. Thus, the total capacitance of the cubic unit will be

$$C_{unit} = \frac{C_{layer_1} \cdot C_{layer_2}}{C_{layer_1} + C_{layer_2}} \tag{5.25}$$

$$= \frac{4\varepsilon_r r[2\pi r\varepsilon_0\varepsilon_r \ln(\varepsilon_r) + \varepsilon_0(\varepsilon_r - 1)(4 - \pi)r]}{2\pi r\varepsilon_r(d - r)\ln(\varepsilon_r) + (d - r)(4 - \pi)(\varepsilon_r - 1) + 4\varepsilon_r r(\varepsilon_r - 1)}$$

Therefore, the electrostatic force drop ratio can be easily calculated by

$$\eta = \frac{F_{electr}}{F_{orignial}} = \frac{\frac{(\sum C_{unit})V^2}{2d}}{\frac{C_{original}V^2}{2d}} = \frac{C_{unit}}{C_{cube}} \tag{5.26}$$

$$= \frac{\frac{4\varepsilon_r r[2\pi r\varepsilon_0\varepsilon_r \ln(\varepsilon_r)+\varepsilon_0(\varepsilon_r-1)(4-\pi)r]}{2\pi r\varepsilon_r(d-r)\ln(\varepsilon_r)+(d-r)(4-\pi)(\varepsilon_r-1)+4\varepsilon_r r(\varepsilon_r-1)}}{\frac{4\varepsilon_0\varepsilon_r r^2}{d}}$$

$$= \frac{d[2\pi\varepsilon_r \ln(\varepsilon_r) + (\varepsilon_r - 1)(4-\pi)]}{2\pi\varepsilon_r(d-r)\ln(\varepsilon_r) + (d-r)(4-\pi)(\varepsilon_r - 1) + 4\varepsilon_r r(\varepsilon_r - 1)}$$

For instance, a RF switch with its contacting area of $120\times 80\mu m^2$ and the thickness of $0.4\mu m$, and $r = 0.2\mu m$, with a membrane made of gold, and the dielectric layer composed of silicon dioxide ($\varepsilon_r = 5.5$), we have

$$\eta = \frac{0.4[2\pi\times 5.5\times \ln(5.5) + (5.5-1)(4-\pi)]}{2\pi\times 0.2\times 10^{-6}\times 5.5\times(0.4-0.2) + (0.4-0.2)\times(4-\pi)\times(\varepsilon_r - 1) + 4\times 5.5\times 0.2\times(5.5-1)}\times 100\% = 77.6\%$$

Moreover, by removing the amount of the semispheres in the array, we could reduce the capacitance of the switch, which will results in a further reducing of the ratio η, so that we can diminish the electrostatic force caused by the dielectric charging.

Fig.5-20 and Fig.5-21 show some nanoscale structures fabricated by FIB (these nanostructures were fabricated by the author during his undergraduate period). By employing FIB machining, we can easily use grey image to design the desired structures and attain modifying the geometry of the dielectric layer.

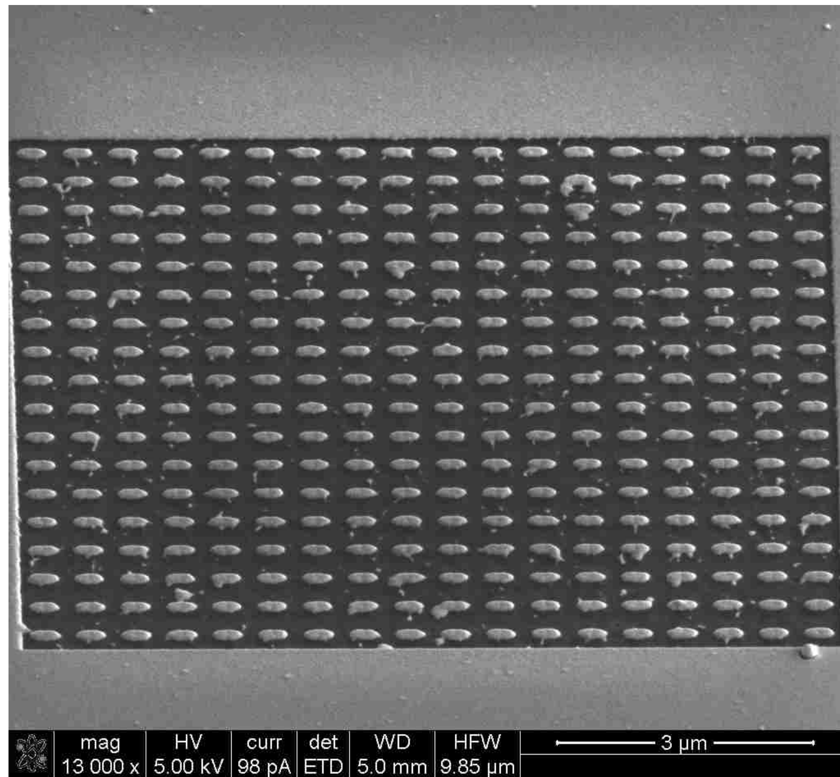

Fig.5-20 SEM micrograph of FIB machining cylindroid array

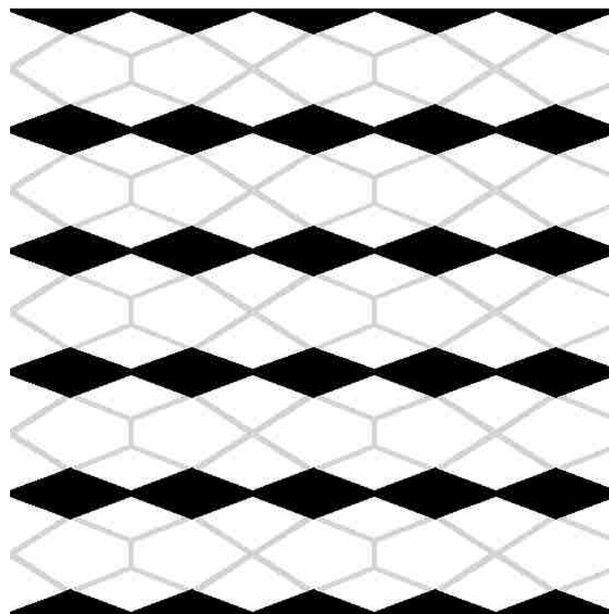

(a)

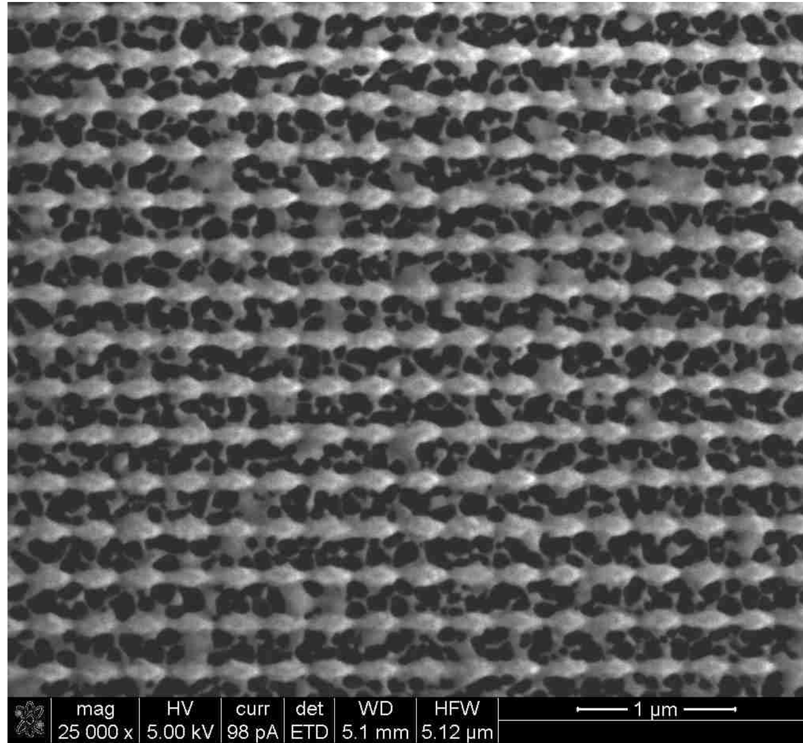

(b)

Fig.5-21 (a) the grey image used for NOVA200 to fabricate the nanostructure; (b) SEM of web-shaped rhombic array.

However, we attain reducing the electrostatic force at the expense of reducing the capacitance. For instance, for corrugation profile, when we reduce the electrostatic force caused by the dielectric charging to ηF, the capacitance reduce to ηC as well. It seems very contradictory. On one hand, when we decrease the contacting area, we could successfully reduce the capillary force, Van der Waals force, and electrostatic force; on the other hand, a small capacitance will result in a higher pull-in voltage, which in turn may increase the power consumption of the whole system. Moreover, such low capacitance may not be suitable for many applications.

Therefore, how to modify the dielectric geometry in order to reduce the dielectric charging effect and humidity effect, while obtain an acceptable pull-in voltage and capacitance is still an unresolved issue for the future designers.

6 Conclusion and Future Work

This study mainly focuses on the simulation of the RF MEMS switch. As the most critical component in RF MEMS devices, the longevity and stability of this microsystem strongly depends on the performance of the switch. Thus, the investigation of how to improve the behavior and performance becomes an important topic for researchers.

According to previous research on RF MEMS switches, the stiction effect is one overarching factor that affects the electrical and mechanical properties of the switch. In such circumstances, researchers use diverse models to deal with this problem. Basically, these numerous models can be placed into two categories. 1) Modification of the structure, or the material properties, of the membrane and the dielectric layer, so that one can attain decreased dielectric charging; 2) employing some outer means, e.g., decrease the environment temperature to increase the restoring force of the membrane.

In our case, we choose the second method to overcome the stiction effect. In our opinion, by manipulating the temperature of the membrane, we could obtain a desired thermal stress to enhance the restoring force. Therefore, we employ ANSYS here to model the relationship between temperature and the thermal stress.

As the thickness of the membrane is much smaller than its width, we first ignore its width and assume that it`s a 2-D problem with infinite width. After obtaining the temperature-stress curve, we move to the 3-D model to demonstrate the accuracy of

the 2-D model. From the 3-D simulation, we can see that the 2-D model basically matches the 3-D FEA simulation. And from the results we can also find out that, the restoring force has a trend to increase with the decreasing temperature.

Moreover, based on the information we obtained, we can further calculate the electrostatic force and electrostatic potential generated by the dielectric charging, so that we can obtain the relationship between release voltage and temperature. As the release voltage is a critical parameter in estimating the performance of the RF MEMS switch, this FEA simulation provides us a simple way to obtain the release voltage under various temperatures. We could even use the electrostatic potential generated by the dielectric charging to estimate the degree of the dielectric charging, and obtain an approximately estimation of the charge density under certain temperature. Therefore, we relate the charge density to the environment temperature.

However, there are still many problems waiting to be solved.

(1) How to determine the critical release force, $F_{release}$. As we defined earlier, the release force occurs when the membrane is about to spring back to its initial position, which means we should find out the exact time when the supporting force offered by the dielectric layer disappears. This will be more complicated to use ANSYS to simulate, as it includes the modeling of electrical field, thermal field, and structural field. Find out an accurate model to simulate such particular problem is a valuable work in our future study.

(2) Although, decreasing the temperature to a certain value will help increasing the restoring force in the membrane, a too low temperature may also increase the

pull-in voltage of the RF MEMS switch, which will lead to additional power consumption. On the contrary, The RF switches working in a high temperature environment will make an irreversible damage to the RF switches. Thus, how to control the temperature within an acceptable range should be considered carefully by us.

(3) By calculating the reduction ratio with different design of dielectric layer geometry, we can find out the effect of these geometries on the switch behavior. However, how to balance the reduction of electrostatic force caused by the charging effect and the commercial requirement is still an important issue that needs to be considered.

Appendix

According to Ref.[57], we could find out the elastic modulus under different temperatures. However, as the data show in Table.App-1, the values we need are not listed. Here, we can employ invariance theorem to interpolate the values we need in the diagraph.

Table.App-1Elastic Modulus

Temperature (℃)	Elastic Modulus (GPa)
23	76.661
35	76.559
79	75.308
92	74.945
128	73.795
167	72.764
193	72.116
225	71.293

Invariance Theorem [63]:

The divided difference $f[x_0, x_1, x_2, \dots, x_k]$is invariant under all permutations of the arguments $x_0, x_1, x_2, \dots, x_k$. And the recursive formulation can be written as

$$f\left[x_i, x_{i+1}, \dots, x_{j-1}, x_j\right] = \frac{f\left[x_{i+1}, x_{i+2}, \dots, x_j\right] - f\left[x_i, x_{i+1}, \dots, x_{j-1}\right]}{x_j - x_i}$$

Following this rule, we can calculate the curve consisted by the data from Table.App-1.

Table.App-2 Calculation of coefficients of polynomial

x	$f(x_i)$	$f(x_{i+1}, x_i)$	$f(x_{i+2}, x_{i+1}, x_i)$
23	76.661	$-8.3*10^{-3}$	$-3.56*10^{-4} \approx 0$
35	76.559	$-2.84*10^{-2}$	$1.23*10^{-5} \approx 0$
79	75.308	$-2.77*10^{-2}$	$8.57*10^{-5} \approx 0$
92	74.945	$-3.19*10^{-2}$	$-6.93*10^{-5} \approx 0$
128	73.795	$-2.67*10^{-2}$	$-6.15*10^{-5} \approx 0$
167	72.764	$-2.77*10^{-2}$	$8.28*10^{-5} \approx 0$
193	72.116	$-2.75*10^{-2}$	
225	71.293		

Now we select the highlighted data to construct the polynomial to approach Table.App-1.

$$p(x) = 76.56 - 0.0284(x - 35)$$

Now we use Matlab to compare the data listed in Table.App-1 with p(x).

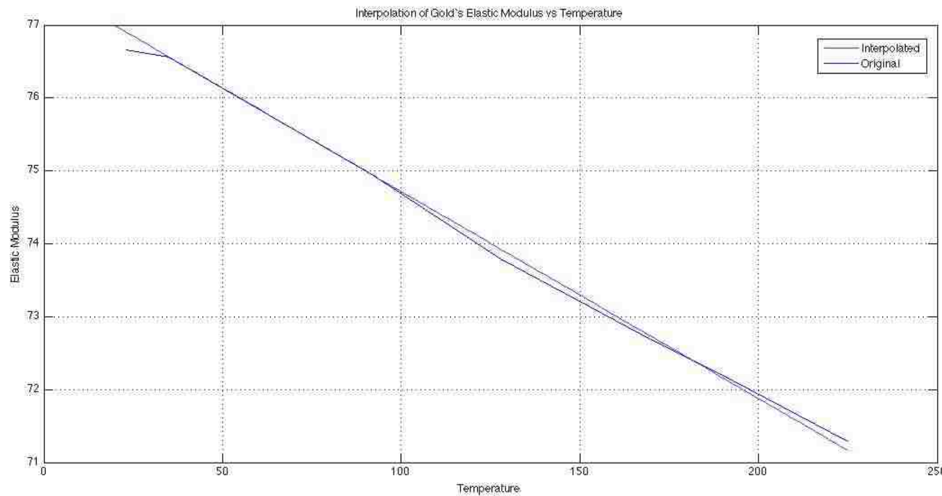

Fig.App Interpolation of desired values

We can see that, the polynomial greatly matches the original data. Therefore, we can use p(x) to solve for the elastic modulus at the desired temperature. As listed in Table.5-2.

Reference

[1] H. Baltes, O. Brand, G. K. Fedder, C. Hierold, J. G. Korvink, and O. Tabata, CMOS MEMS: Advanced Micro and Nanosystems, WILEY-VCH Verlag GmbH & Co. KGaA, Weinheim, 2005

[2] H. Fecht, and M. Werner, Micro Nano interface, Bridging the Micro and Nano Worlds, 2004

[3] J. Ramsden, Applied Nanotechnology, Elsevier Inc., 2009

[4] Z. Cui, Micro/Nanofabrication Technologies and Applications, Springer Science + Business Media, Inc., 2006

[5] A. A. Tseng, Nanofabrication: fundamentals and applications, World Scientific Publishing Co. Pte. Ltd., 2008

[6] L. A. Giannuzzi, and F. A. Stevie, Introduction to Focused Ion Beams: Instrumentation, Theory, Techniques, and Practice, Springer Science + Business Media, Inc., 2005

[7] C. Liu, Foundations of MEMS, Pearson Prentice Hall, 2005

[8] Z. Y. Wang, Microsystem Design and Fabrication, Tsinghua University Publisher, 2008

[9] K. E. Petersen. Micromechanical membrane switches on silicon. IBM J Res Dev, 23: 376-385, 1979

[10] G. M. Rebeiz, RF MEMS Theory, Design and Technology. Hoboken, NJ: Wiley, 2003

[11] P. M. Zavracky, S. Majumdar, and N. McGruer, Micromechanical switches fabricated using nickel surface micromachining, Journal of Microelectromechanical systems 6(1): 3–9, 1997

[12] A. B. Yu, RF MEMS Switches and Integrated Switching Circuits, Design, Fabrication and Test, Springer Science + Business Media LLC, 2010

[13] Y. Wang, et al, A low-voltage lateral MEMS switch with high RF performance. J MEMS, Vol.3, pp.902-911, 2004

[14] J. A. Wright, and Y. C. Tai, Magnetostatic MEMS relays for the miniaturization of brush- less DC motor controllers, Tech. Digest, 12th IEEE Int. Conf. on Microelectromechanical Systems, Orlando Florida, USA, pp. 594–599, 1999

[15] W. P. Taylor, M. G. Allen, Integrated magnetic microrelays: normally open, normally closed, and multi-pole devices, In: Transducers, pp.1149-1152, 1997

[16] H. A. C. Tilmanset al., A fully-packaged electromagnetic microrelay, Tech. Digest. 12th IEEE Int. Conf. on Microelectromechanical Systems, Orlando Florida, USA, pp. 25–30, 1999

[17] H. Hosaka, K. Kuwano, and K. Yanagisawa, Electromagnetic microrelays: concepts and fundamental characteristic, Sensor. Actuator. A Vol. 40, pp. 41–47, 1994

[18] K. E. Petersen. Dynamic micromechanics on silicon: techniques and devices, IEEE Trans. Electron Devices, Vol. ED-25, pp.1241–1250, 1978

[19] M. A. Gr´etillat, F. Gr´etillat, and N. F.de Rooij, Micromechanical relay with electrostatic actuation and metallic contacts, J. Micromech. Microeng. Vol. 9, pp. 324–331, 1999

[20] D Hah, A low-voltage actuated micromachined microwave switch using torsion springs and leverage, IEEE T MTT, Vol.48, pp.2540-2545, 2000

[21] I. J. Cho, T. Song, S.-H. Baek, and E. Yoon, A Low-Voltage and Low-Power RF MEMS Series and Shunt Switches Actuated by Combination of Electromagnetic and Electrostatic Forces, IEEE T MTT, Vol.53, pp.2450-2457, 2000

[22] J.J. Yao, M. F. Chang, A surface micromachined miniature switch for telecommunications applications with signal frequencies from DC up to 4 GHz, Tech. Digest, 8th Int. Conf. on Solid-State Sensors and Actuators,pp.384-387, 1995

[23] C. L. Goldsmith, T. H. Lin, B. Powers, W. R. Wu, B. Norvell, Micromechanical membrane switches for microwave applications, Tech. Digest, IEEE Microwave Theory and Techniques Symp, pp.91-94, 1995

[24] A. Repchankova, Anti-Stiction And Self-Recovery Active Mechanisms For High Reliability RF-MEMS Switches, PhD dissertation, University of Trento, Italy, 2010

[25] Z. Peng, D. Molinero, C. Palego, and James C. M. Hwang, Effect of Surface Conduction on Dielectric Charging in RF MEMS Capacitive Switches, 2010 IEEE

MTT-S International Microwave Symposium Digest, pp.1250-1253, 2010

[26] Z. Peng, X.B. Yuan, James C. M. Hwang, D. Forehand, and C. L. Goldsmith, Top vs. Bottom Charging of the Dielectric in RF MEMS Capacitive Switches, Asia-Pacific Microwave Conference, pp.1535-1538, 2006

[27] X.B. Yuan, James C. M. Hwang, D. Forehand, and C. L. Goldsmith, Modeling and Characterization of Dielectric-Charging Effects in RF MEMS Capacitive Switches, 2005 IEEE MTT-S International Microwave Symposium Digest, pp.753-756, 2005

[28] Z. Peng, C. Palego, James C. M. Hwang, D. I. Forehand, C. L. Goldsmith, C. Moody, A. Malczewski, B. W. Pillans, R. Daigler, and J. Papapolymerou, Impact of Humidity on Dielectric Charging in RF MEMS Capacitive Switches, IEEE Microwaves and Wireless Components Letters, Vol.19(5), pp.299-301, 2009

[29] V. K. Varadan, K. J. Vinoy, K. A. Jose, RF MEMS and their Applications, John Wiley & Sons Ltd, 2003

[30] Y Zhu, H. D. Espinosa, Reliability of capacitive RF MEMS switches at high and low temperatures, International Journal of RF and Microwave Computer-Aided Engineering, Vol.14(4), pp.317-328, 2004

[31] R. V. Sabariego, J. Gyselinck, P. Dular, J. De Coster, F. Henrotte3, K. Hameyer, Coupled Mechanical-electrostatic FE-BE Analysis with FMM Acceleration Application to a Shunt Capacitive MEMS Switch, COMPEL Vol.23 pp.876–884, 2004

[32] W. Weaver, Jr., S. P. Timoshenko, and D. H. Young, Vibration Problems in Engineering, 5th edition, John Wiley & Sons, New York, 1990

[33] MSC Software Corporation, Palo Alto, CA94306

[34] W. S. Griffen, H. H. Richardson, and S. Yamanami, A study of fluid squeeze-film damping, J. Basic Eng. Trans. ASME, pp. 451–456, 1966.

[35] J. J. Blech, On Isothermal Squeeze Films, J. Lubrication Tech., Vol. 105, pp. 615–620, October 1983.

[36] C. L. Goldsmith, D. I. Forehand, Z. Peng, J. C. M. Hwang, and J. L. Ebel, High-cycle life testing of RF MEMS switches, IEEE MTT-S Int. Microwave Symp. Dig., pp.1805-1808, 2007

[37] B. Pillans, L. Coryell, A. Malczewski, C. Moody, F. Morris, and V. Pillai, RF MEMS phase shifters manufacturing technology, Proc. Defense Manufacturing Conf., 2008

[38] Z. Peng, C. Palego, J. C. M. Hwang, D. I. Forehand, C. L. Goldsmith, C. Moody, A. Malczewski, B. W. Pillans, R. Daigler, J. Papapolymerou, Impact of Humidity on Dielectric Charging in RF MEMS Capacitive Switches, IEEE Microwave and wireless components letters, vol.19, no.5, pp.299-301, 2009

[39] L. Mercado, S. M. Kuo, T. Y. Lee, L. J. Liu, A Mechanical Approach to Overcome RF MEMS Switch Stiction Problem, Electronic Components and Technology Conference, pp.337-384

[40] A. B. Yu, A. Q. Liu, J. Oberhammer, Q. X. Zhang, and H. M. Hosseini, Characterizationand optimization of dry releasing for the fabrication of RF MEMS capacitive switches, J. Micromech. Microeng. Vol. 17, pp. 2024–2030, 2007

[41] L.L. Mercado, T.Y.T. Lee, S.M. Kuo, and C. Amrine, Thermal solutions for discrete and wafer-level RF MEMS switch packages, IEEE Trans Adv Packaging, Vol.26, 318–326, 2003

[42] B.R. Norvell, R.J. Hancock, J.K. Smith, M.L. Pugh, S.W. Theis, and J. Kviatkofsky, Micro Electro Mechanical Switch (MEMS) technology applied to electronically scanned arrays for space based radar, IEEE Aerospace Conf, Aspen, CO, pp. 239–247, 1999

[43] Y Zhu, H. D. Espinosa, Effect of temperature on capacitive RF MEMS switch performance—a coupled-field analysis, J. Micromech. Microeng. Vol.14, pp.1270–1279, 2004

[44] C. L. Goldsmith, J. Ehmke, A. Malczewski, B. Pollans, S. Eschelman, Z. Yao, J. Brank, and M. Eberly, Life Time Characterization of Capacitive RF MEMS Switches IEEE MTT-S Int. Microwave Symp. Digest pp.227–30, 2001

[45] X. Lafontan, C. Le Touze, B. Wenk, I. Kolesnik, F. Pressecq, G. Perez, J M. Nicot,

M. Dardalhon, and S. Rigo, Environmental Test Bench for Reliability Studies: Influence of the Temperature on RF Switches with Metallic membranes, J of Design, Test, Integration, and Packaging of MEMS/MOEMS, vol. 4755, pp.624-633, 2002

[46] J. B. Rizk, E. Chaiban, and G. M. Rebeiz, Steady state Thermal Analysis and High-power Reliability Considerations of RF MEMS Capacitive Switches, IEEE MTT-S Digest, pp.239–42, 2002

[47] X. Chauffleur, L. Rabbia, P. Pons, K. Grenier, R. Plana, and L. Dantas, Effect of Membrane Shape on Mechanical Behavior of RF Switches Tech. Digest, 16th Euro. Conf. on Solid-State Transducers,pp.92–5, 2002

[48] J. L. Nowinski, Theory of Thermoelasticity with Application, Sijthoff and Noordhoff International Publishers,1978

[49]N. Noda, R. B. Hetnarski, Y. Tanigawa, Thermal Stresses, Taylor& Francis, 2002

[50] A.E. Green, K. A. Lindsay, Thermoelasticity, Journal of Elasticity, p.1-7, 1971

[51] S. Jiang, R. Racke, Evolution Equations in Thermoelasticity, CRC Press LLC, 2000

[52] W. A. Day, Heat Conduction within Linear Thermoelasticity, Springer-Verlag, 1985

[53] S. Moaveni, Finite Element Analysis, Theory and Application with ANSYS, Pearson Prentice Hall, 2008

[54] A. Witvrouw, H.A.C. Tilmans, I. De Wolf, Materials issues in the processing, the operation and the reliability of MEMS, Microelectronic Engineering, Vol.76, pp.245–257, 2004

[55] A. Bogozi, Elastic constant of silver and gold, PhD dissertation, Florida International University, 2005

[56] S. M. Collard, High-temperature Elastic constant of Gold-crystal, PhD dissertation, Rice University, 1991

[57] E. Madenci, and I.Guven, The Finite Element Method and Applications in Engineering Using ANSYS, Springer Science + Business Media LLC, 2005

[58] Y. Nakasone, T. A. Stolarski, and S. Yoshimoto, Engineering Analysis with ANSYS software, MPG Books Ltd., 2006

[59] C. L. Goldsmith, D.I. Forehand, Z. Peng, J.C.M. Hwang, and J.L. Ebel, High-Cycle Life Testing of RF MEMS Switches, 2007 IEEE MTT-S International Microwave Symposium, pp.1085-1088, 2007

[60] P.D. Bisio, J.G. Cartledge, W.H. Keesom, C.J. Radke, Molecular Orientation of Aqueous Surfactants on A Hydrophobic Solid, Journal of Colloid and Interface Science, Vol.78(1), pp.225-234, 1980

[61] P. H. Blustin, A Floating Gaussian Orbital Calculation on Argon Hydrochloride (ArHCl), Theoret. Chim. Acta., Vol.37, pp.249-257, 1978

[62] F. London, The General Theory of Molecular Force, Trans. Faraday Soc., 33, 8b-26, 1936

[63] W. Cheney, D. Kincaid, Numerical mathematics and computing, Thomson Books/Cole, 2007

Vita

Guosong Zeng was born on August 15, 1987, in Guilin, China. He graduated from Foreign Language School Attached to Guangxi Normal University in 2006. He was accepted by Tianjin University after that, and obtained his baccalaureate in Measuring and Control Technology and Instruments in 2010.

He came to the U.S. at August 2010, and pursues his master degree in the field of Mechanical Engineering in Lehigh University. He expects to obtain his degree of M.S. at May 2012.